

# Ruthenium–Cobalt Mixed-Metal Nitrido and Nitrene Carbonyl Clusters: Structure, Reactivity, and $^{15}\text{N}$ NMR Spectroscopy

Emmie Ngai-Man Ho,<sup>[a]</sup> Zhenyang Lin,<sup>[b]</sup> and Wing-Tak Wong\*<sup>[a]</sup>

**Keywords:** Electrochemistry / NMR spectroscopy / Nitrides / Nitrenes / Ruthenium / Cobalt / Cluster compounds

The reaction of  $[\text{Ru}_3(\mu\text{-H})_2(\text{CO})_9(\mu_3\text{-NOMe})]$  (**1**) with  $[\text{Cp}^*\text{Co}(\text{CO})_2]$  ( $\text{Cp}^* = \eta^5\text{-C}_5\text{Me}_5$ ) in refluxing THF afforded the new clusters  $[\text{Ru}_3\text{Co}(\mu\text{-H})(\text{CO})_9(\eta^5\text{-C}_5\text{Me}_5)(\mu_4\text{-N})]$  (**2**),  $[\text{Ru}_2\text{Co}(\text{CO})_6(\mu_3\text{-CO})(\eta^5\text{-C}_5\text{Me}_5)(\mu_3\text{-NH})]$  (**3**),  $[\text{Ru}_5(\mu\text{-H})(\text{CO})_9(\mu\text{-CO})_3(\eta^5\text{-C}_5\text{Me}_5)(\mu_4\text{-NH})]$  (**4**), and  $[\text{Ru}_6\text{Co}(\mu_3\text{-H})(\text{CO})_8(\mu\text{-CO})_3(\mu_4\text{-}\eta^2\text{-CO})(\eta^5\text{-C}_5\text{Me}_5)_3(\mu_4\text{-N})]$  (**5**). Clusters **2** and **3** have typical butterfly nitrido and triangular nitrene structures, whilst compound **4** is a novel square-pyramidal pentaruthenium  $\mu_4\text{-NH}$  carbonyl cluster with a  $\text{Cp}^*$  ligand transferred from the external mononuclear Co complex. Cluster **4** can also be obtained by the reaction of **1** with pentamethylcyclopentadiene in the presence of 1,3-cyclohexadiene, albeit in low yield. Compound **5** consists of a rare  $\text{Ru}_6\text{Co}$  metal framework where a basal Ru–Ru edge of the central  $\text{Ru}_4$  tetrahedron is capped by a  $\text{Cp}^*\text{Co}$  fragment and another edge is bridged by a diruthenium unit. Complex **2** was found to be converted into **3** upon deprotonation with 1,8-diazabicyclo[5.4.0]undec-7-ene, on refluxing with  $[\text{Cp}^*\text{Co}(\text{CO})_2]$ , or on exhaustive electrolysis. Upon thermolysis of **2** with  $\text{PhC}_2\text{Ph}$  in *n*-octane,  $[\text{Ru}_3\text{Co}(\text{CO})_6(\mu\text{-CO})_2(\eta^5\text{-C}_5\text{Me}_5)(\mu_4\text{-NH})(\mu_4\text{-}\eta^2\text{-PhC}_2\text{Ph})]$  (**6**) and  $[\text{Ru}_3\text{Co}(\text{CO})_5(\mu\text{-CO})_2(\eta^5\text{-C}_5\text{Me}_5)(\mu_4\text{-}\eta^3\text{-}$

$\text{NC}(\text{O})\text{C}_2(\text{C}_4\text{H}_4)\text{CHCH}(\text{Ph})](\mu_4\text{-}\eta^2\text{-PhC}_2\text{Ph})]$  (**7**) were obtained in moderate yields. The structures of **6** and **7** both consist of a slightly twisted  $\text{Ru}_3\text{Co}$  square base with a quadruply bridging  $\text{PhC}_2\text{Ph}$  ligand. Cluster **6** is capped by a  $\mu_4\text{-NH}$  moiety on the opposite side, while in **7** a CO ligand and an *ortho*-carbon atom of a Ph group from another  $\text{PhC}_2\text{Ph}$  ligand interact with the  $\mu_4\text{-N}$  nitrido atom. Molecular orbital calculations have been carried out in order to gain further insight into the electronic structures of these interesting square-planar  $\text{Ru}_3\text{Co}$  and  $\text{Ru}_4$  clusters. The butterfly  $\text{Ru}_2\text{Co}_2$  nitrido complex  $[\text{Ru}_2\text{Co}_2(\text{CO})_9(\eta^5\text{-C}_5\text{Me}_5)(\mu_4\text{-N})]$  (**8**) was isolated from the reaction of  $[\text{Ru}_3\text{Co}(\text{CO})_{12}(\mu_4\text{-N})]$  with  $[\text{Cp}^*\text{Co}(\text{CO})_2]$  in refluxing THF as a result of metal exchange of an  $\text{Ru}(\text{CO})_3$  fragment by a  $\text{Cp}^*\text{Co}$  moiety. The redox properties of the compounds described herein have been investigated by means of cyclic voltammetry and controlled potential coulometry. Cluster **6** was shown to be able to tolerate both the addition of two electrons and the removal of one electron without significant structural change. The chemical environments of the nitrogen atoms of these clusters have been investigated by analysis of their  $^{15}\text{N}$  NMR chemical shifts.

## Introduction

Nitrido and nitrene clusters are members of a potentially vast class of mixed transition metal–main group compounds. Such molecules are currently of structural and chemical interest<sup>[1–9]</sup> since they offer opportunities to evaluate the validity of current models of bonding for mixed polynuclear systems and to improve on the degradative instability of homonuclear metal compounds. Metal surface-bound nitrido and nitrene species are believed to be central to a number of heterogeneously catalysed chemical processes such as nitrogen oxide reduction, the Haber process, and hydrazine decomposition.<sup>[10]</sup> In several surface reactions involving NO or  $\text{N}_2$ , adsorbed nitrogen atoms are known to be key intermediates. In the case of the Haber process, the mechanism is believed to involve formation of the metal nitride followed by successive additions of hydrogen atoms to the nitrogen giving ammonia.<sup>[11]</sup> In view of the

metal cluster–metal surface analogy,<sup>[12]</sup> chemical reactivity studies of low-valent nitrido and nitrene are of considerable interest.

The chemistry of the triruthenium carbonyl methoxynitrido clusters  $[\text{Ru}_3(\text{CO})_9(\mu_3\text{-CO})(\mu_3\text{-NOMe})]$  and  $[\text{Ru}_3(\mu\text{-H})_2(\text{CO})_9(\mu_3\text{-NOMe})]$  (**1**) has been described in previous papers by ourselves and others.<sup>[13–19]</sup> These two methoxynitrido clusters were reported to be synthetic precursors for nitrido and nitrene species such as  $[\text{Ru}_4(\text{CO})_{12}(\mu_4\text{-N})(\mu\text{-OMe})]$ ,  $[\text{Ru}_6(\text{CO})_{13}(\mu\text{-CO})(\mu_5\text{-N})(\mu_3\text{-NH})(\mu_3\text{-OMe})\{\mu\text{-}\eta^2\text{-C}(\text{O})\text{OMe}\}_2]$ , and  $[\text{Ru}_6(\text{CO})_{16}(\mu\text{-CO})_2(\mu_4\text{-NH})(\mu\text{-OMe})(\mu\text{-R})]$  (where  $\text{R} = \text{H}$ ,  $\text{OMe}$ , or  $\text{NCO}$ ),<sup>[15–17]</sup> albeit giving only low yields ( $\approx 5\%$ ). A series of nitrene clusters containing alkyne ligands,  $[\text{Ru}_4(\text{CO})_9(\mu\text{-CO})_2(\mu_4\text{-NR})(\mu_4\text{-}\eta^2\text{-PhC}_2\text{R}')]$  [ $\text{R} = \text{H}$ ,  $\text{OMe}$ , or  $\text{C}(\text{O})\text{OMe}$ ;  $\text{R}' = \text{H}$  or  $\text{Ph}$ ], was obtained in more acceptable yields from reactions of  $[\text{Ru}_3(\text{CO})_9(\mu_3\text{-CO})(\mu_3\text{-NOMe})]$  with alkynes.<sup>[13,14]</sup> It is suspected that the formation of nitrido ligands, and hence of nitrene ligands as well, involves initial N–O bond scission of the methoxynitrido ligand. In the formation of these polynuclear  $\mu_4\text{-nitrido}$  or  $\mu_4\text{-NR}$  species, coupling reactions of the methoxynitrido clusters such as  $[\text{Ru}_3(\text{CO})_9(\mu_3\text{-CO})(\mu_3\text{-NOMe})]$  or **1** with other organometallic moieties (another molecule of a methoxynitrido cluster or some degraded

<sup>[a]</sup> Department of Chemistry, The University of Hong Kong, Pokfulam Road, Hong Kong, P. R. China  
Fax: (internat.) + 852/25472933 or 28571586  
E-mail: wtwong@hkucc.hku.hk

<sup>[b]</sup> Department of Chemistry, The Hong Kong University of Science and Technology, Clear Water Bay, Kowloon, Hong Kong, P. R. China

ruthenium carbonyl fragments) is invariably accompanied by N–O bond cleavage. In order to generate some nitrido or nitrene clusters and to study the underlying mechanisms of their formation, methods allowing the incorporation of different external organometallic fragments would be desirable.

Mixed-metal clusters are potential precursors to supported bimetallic catalysts. Moreover, the different metals provide effective labels for ligand fluxionality studies, and varying the metals of the cluster core offers the possibility of metallo- and bond-selectivity and thus of directing reactivity for a range of reagents. Mixed ruthenium–cobalt systems are especially attractive because of the significance of these metals in CO chemistry, e.g. in the catalysis of CO hydrogenation,<sup>[20,21]</sup> and in the homologation of alcohols<sup>[22–24]</sup> and esters.<sup>[25,26]</sup> More recently, Ru/Co mixed-metal clusters have been used as precursors to generate nanoparticles with unusual magnetic properties.<sup>[27]</sup> The reactions of  $[\text{Ru}_3(\text{CO})_9(\mu_3\text{-CO})(\mu_3\text{-NOMe})]$  with  $[(\eta^5\text{-C}_5\text{H}_5)\text{Mo}(\text{CO})_3\text{H}]/[\{(\eta^5\text{-C}_5\text{H}_5)\text{Mo}(\text{CO})_3\}_2\text{Hg}]$  have been studied.<sup>[28]</sup> However, neither the nitrene nor the nitrido species were isolated. In this paper, we report on an initial study of the syntheses, characterization, electrochemical properties, and structures of a series of ruthenium–cobalt mixed-metal nitrido and nitrene carbonyl clusters obtained by addition of Co mononuclear complexes to clusters **1** and  $[\text{Ru}_3\text{Co}(\text{CO})_{12}(\mu_4\text{-N})]$ , as well as on  $^{15}\text{N}$  NMR spectroscopic studies of the nitrido/nitrene ligands in these clusters.

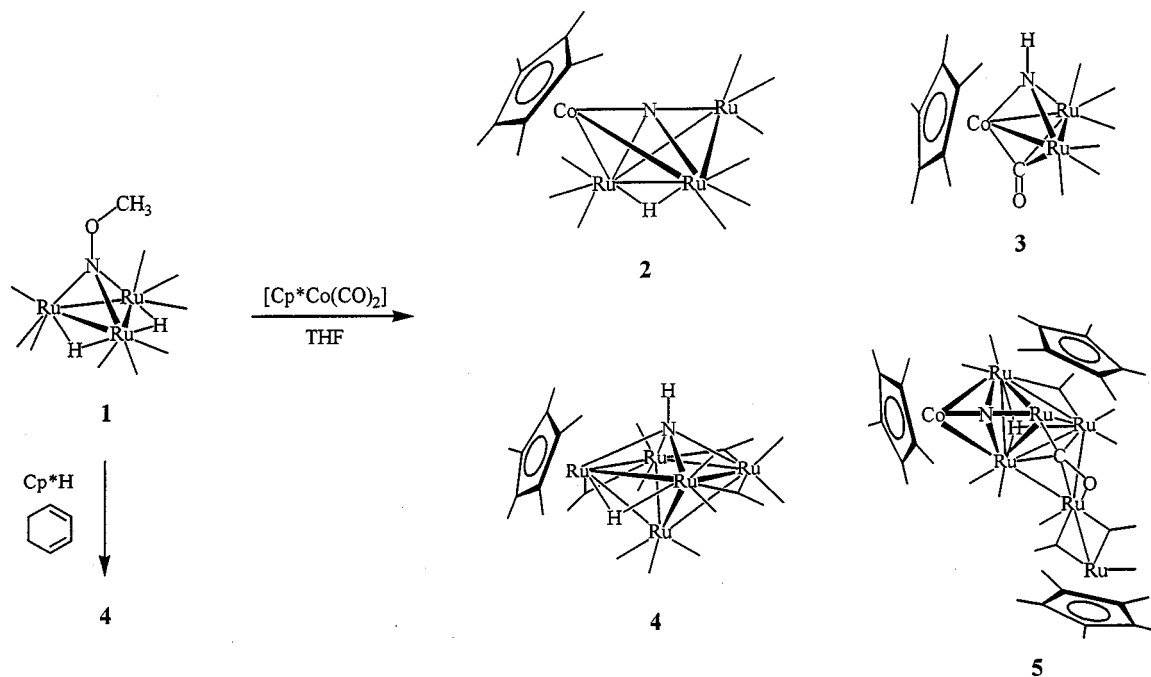
## Results and Discussion

### Synthesis and Characterization

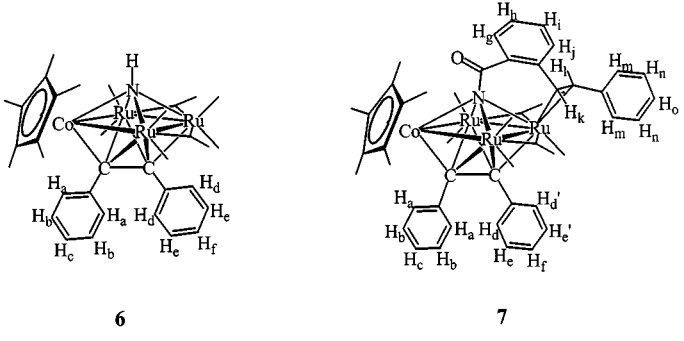
#### Reaction of $[\text{Ru}_3(\mu\text{-H})_2(\text{CO})_9(\mu_3\text{-NOMe})]$ (**1**) with $[\text{Cp}^*\text{Co}(\text{CO})_2]$

A solution of  $[\text{Ru}_3(\mu\text{-H})_2(\text{CO})_9(\mu_3\text{-NOMe})]$  (**1**) and  $[\text{Cp}^*\text{Co}(\text{CO})_2]$  in THF becomes almost black upon refluxing over a period of 10 h. Subsequent chromatographic separation of the product mixture gives, in order of elution, brown  $[\text{Ru}_3\text{Co}(\mu\text{-H})(\text{CO})_9(\eta^5\text{-C}_5\text{Me}_5)(\mu_4\text{-N})]$  (**2**, 55%), trace amounts of starting material  $[\text{Ru}_3(\mu\text{-H})_2(\text{CO})_9(\mu_3\text{-NOMe})]$  (**1**) and the known compound  $[\text{Ru}_3(\mu\text{-H})(\text{CO})_9(\mu_3\text{-NH})]$  (**3**, 20%), purple  $[\text{Ru}_2\text{Co}(\text{CO})_6(\mu_3\text{-CO})(\eta^5\text{-C}_5\text{Me}_5)(\mu_3\text{-NH})]$  (**4**, 3%), and red  $[\text{Ru}_5(\mu\text{-H})(\text{CO})_9(\mu\text{-CO})_3(\eta^5\text{-C}_5\text{Me}_5)(\mu_4\text{-NH})]$  (**5**, 2%) (Scheme 1). The structures of clusters **2–5** were unambiguously established by single-crystal X-ray crystallography and were supported by  $^1\text{H}$  and  $^{15}\text{N}$  NMR, IR, and UV/vis spectroscopic data, as well as by FAB mass spectrometry (Table 1). These compounds are essentially air-stable in the solid state, have varying degrees of stability in solution, and are all soluble in *n*-hexane.

Cluster **2** readily crystallizes from a rich brown-coloured band over a period of a few days. The presence of the  $\text{Cp}^*$  and metal hydride groups in this compound is apparent from its  $^1\text{H}$  NMR spectrum (singlets at  $\delta = 1.98$  and  $-24.40$ ), while the integrals of these resonances reveal a



Scheme 1. Treatment of dihydrido cluster **1** with 2 equiv. of  $[\text{Cp}^*\text{Co}(\text{CO})_2]$  led to the formation of the  $[\text{Ru}_3\text{Co}(\mu\text{-H})(\text{CO})_9(\eta^5\text{-C}_5\text{Me}_5)(\mu_4\text{-N})]$  (**2**),  $[\text{Ru}_2\text{Co}(\text{CO})_6(\mu_3\text{-CO})(\eta^5\text{-C}_5\text{Me}_5)(\mu_3\text{-NH})]$  (**3**),  $[\text{Ru}_5(\mu\text{-H})(\text{CO})_9(\mu\text{-CO})_3(\eta^5\text{-C}_5\text{Me}_5)(\mu_4\text{-NH})]$  (**4**), and  $[\text{Ru}_6\text{Co}(\mu_3\text{-H})(\text{CO})_8(\mu\text{-CO})_3(\eta^5\text{-C}_5\text{Me}_5)_3(\mu_4\text{-N})]$  (**5**) in yields of 55%, 20%, 3%, and 2%, respectively; cluster **4** could be directly synthesized by the reaction of **1** with pentamethylcyclopentadiene and 1,3-cyclohexadiene, albeit in low yield (4%)

Table 1. Spectroscopic data for clusters **1–8** with labelling scheme for  $^1\text{H}$  NMR assignments for clusters **6** and **7**


Cluster	IR spectra <sup>[a]</sup> $\nu(\text{CO}) [\text{cm}^{-1}]$	$^1\text{H}$ NMR spectra <sup>[b]</sup> ( $\delta$ , J/Hz)	$^{15}\text{N}$ NMR spectra <sup>[c]</sup> ( $\delta$ , J/Hz)	Mass spectra <sup>[d]</sup> ( $m/z$ )	$\lambda_{\text{max}}^{[\text{e}]}$ (nm) ( $\epsilon$ , $8^{-3} \text{ dm}^3 \text{ mol}^{-1} \text{ cm}^{-1}$ )
<b>1</b>	2116m, 2078s, 2057vs, 2048s, 2036sh, 2010vs, 2005s, 1988m	3.46 (s, 3 H, ethoxy) −17.22 (s, 2 H, hydride)	301.0 (s) <sup>[f]</sup>	602 (602)	295 (9.13) 397 (1.04) <sup>[g]</sup>
<b>2</b>	2074m, 2047vs, 2033s, 2008vs, 1989m, 1970w	1.98 (s, 15 H, $\text{C}_5\text{Me}_5$ ) −24.40 (s, 1 H, hydride)	481.1 (s)	764 (764)	302 (20.1) 353 (19.6) 430 (5.79) 513 (2.03)
<b>3</b>	2072m, 2045vs, 2024vw, 2005s, 1987m, 1974w	7.46 (t, $J_{\text{NH}} = 54.80$ , 1 H, NH) 1.77 (s, 15 H, $\text{C}_5\text{Me}_5$ )	131.4 [d, $J(^{15}\text{N})\text{H}] =$ 76.95 Hz]	607 (607)	292 (14.3) 405 (3.26) 542 (1.84)
<b>4</b>	2076m, 2039vs, 2016s, 2006m, 1991w, 1976m, 1958w, 1943vw, 1868m, 1839m	6.28 (t, $J_{\text{NH}} = 48.82$ , 1 H, NH) 2.20 (s, 15 H, $\text{C}_5\text{Me}_5$ ) −14.92 (s, 1 H, hydride)	145.4 [d, $J(^{15}\text{N})\text{H}] =$ 68.26 Hz]	992 (992)	330 (6.32) <sup>[g]</sup> 345 (5.66) <sup>[g]</sup> 405 (2.58) <sup>[g]</sup> 466 (1.83)
<b>5</b>	2084vw, 2070vw, 2033m, 2030m, 2018w, 2005m, 1997vs, 1987m, 1979m, 1974m, 1953w, 1937s, 1763m	2.24 (s, 15 H, $\text{C}_5\text{Me}_5$ ) 2.20 (s, 15 H, $\text{C}_5\text{Me}_5$ ) 1.76 (s, 15 H, $\text{C}_5\text{Me}_5$ ) −26.46 (s, 1 H, hydride)	548.8 (s)	1421(1421)	360 (11.1) 390 (9.86) <sup>[g]</sup> 579 (2.40)
<b>6</b>	2059m, 2006vs, 2001m, 1954m, 1873w, 1842m	7.00 (m, 2 H, phenyl $\text{H}_b$ ) 6.85 (tt, $J_{\text{HH}} = 7.36, 1.84$ , 1 H, phenyl $\text{H}_c$ ) 6.70 (m, 2 H, phenyl $\text{H}_a$ ) 6.60 (m, 2 H, phenyl $\text{H}_e$ ) 6.51 (tt, $J_{\text{HH}} = 7.27, 2.23$ , 1 H, phenyl $\text{H}_f$ ) 5.65 (m, 2 H, phenyl $\text{H}_d$ ) 2.76 (t, $J_{\text{NH}} = 49.08$ , 1 H, NH) 1.86 (s, 15 H, $\text{C}_5\text{Me}_5$ )	70.2 [d, $J(^{15}\text{N})\text{H}] =$ 69.26 Hz]	914 (914)	296 (5.60) 330 (5.60) 420 (1.77) 505 (0.88)
<b>7</b>	2089vw, 2066w, 2030w, 2014vs, 2005m, 1962m, 1879w, 1844m	7.45 (m, 1 H, phenyl $\text{H}_g$ ) 7.43 (m, 2 H, phenyl $\text{H}_m$ ) 7.35 (m, 3 H, phenyl $\text{H}_h, \text{H}_n$ ) 7.23 (tt, $J_{\text{HH}} = 7.18, 1.25$ , 1 H, phenyl $\text{H}_o$ ) 7.09 (m, 1 H, phenyl $\text{H}_i$ ) 7.01 (m, 1 H, phenyl $\text{H}_j$ ) 6.93 (m, 2 H, phenyl $\text{H}_b$ ) 6.79 (tt, $J_{\text{HH}} = 7.33, 1.12$ , 1 H, phenyl $\text{H}_c$ ) 6.70 (m, 2 H, phenyl $\text{H}_a$ ) 6.58 (m, 1 H, phenyl $\text{H}_c/\text{H}_c'$ ) 6.50 (m, 1 H, phenyl $\text{H}_c/\text{H}_c'$ ) 6.41 (tt, $J_{\text{HH}} = 7.32, 1.12$ , 1 H, phenyl $\text{H}_f$ ) 5.75 (d, 1 H, $J_{\text{HH}} = 12.26$ , $\text{H}_l$ ) 5.60 (m, 1 H, phenyl $\text{H}_d/\text{H}_d'$ ) 5.54 (m, 1 H, phenyl $\text{H}_d/\text{H}_d'$ ) 2.72 (d, 1 H, $J_{\text{HH}} = 12.26$ Hz $\text{H}_k$ ) 1.54 (s, 15 H, $\text{C}_5\text{Me}_5$ ) 1.89 (s, 15 H, $\text{C}_5\text{Me}_5$ )	—	1092 (1092)	—
<b>8</b>	2072s, 2030vs, 2006s, 1983m, 1970w	1.54 (s, 15 H, $\text{C}_5\text{Me}_5$ ) 1.89 (s, 15 H, $\text{C}_5\text{Me}_5$ )	524.7 (s)	721 (721)	315 (9.13) 360 (7.31) 435 (2.00) <sup>[g]</sup> 520 (0.88)

[a] In *n*-hexane unless otherwise stated. — [b] In  $\text{CD}_2\text{Cl}_2$ . — [c] In  $\text{CDCl}_3$ , with  $^1\text{H}$  decoupled except for clusters **3**, **4**, and **6**. — [d] Calculated values in parentheses. — [e] Measured in  $\text{CH}_2\text{Cl}_2$  at 298 K. — [f] From ref.<sup>[29]</sup> — [g] Shoulder.

ratio of 15:1. The  $^{15}\text{N}$  NMR spectrum features a single resonance at  $\delta = 481.1$ , which is consistent with the presence of a  $\mu_4$ -nitrido ligand. Four electronic absorption bands at 302, 353, 430, and 513 nm are seen in the UV/vis spectrum of **2**. The structure of **2** was confirmed by a single-crystal X-ray diffraction analysis; a molecular drawing is shown in Figure 1. Selected bond lengths and angles are given in Table 2.

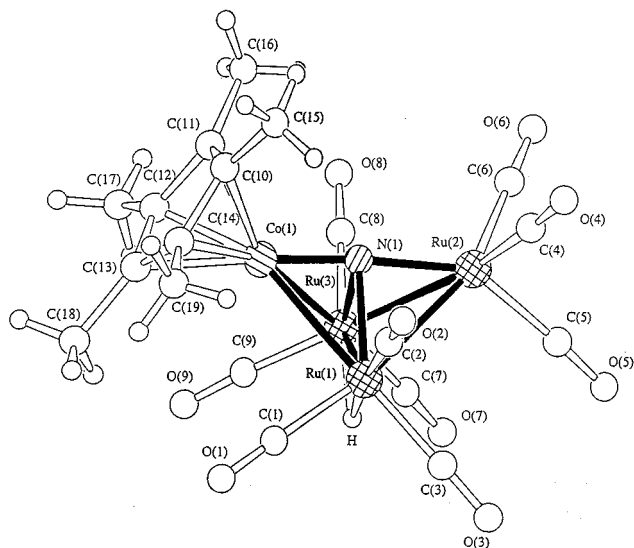


Figure 1. The molecular structure of  $[\text{Ru}_3\text{Co}(\mu\text{-H})(\text{CO})_9(\eta^5\text{-C}_5\text{Me}_5)(\mu_4\text{-N})]$  (**2**) showing the atom numbering scheme

Table 2. Selected bond lengths [Å] and angles [°] for clusters **2** and **8**

	<b>2</b>	<b>8</b>
Ru(1)–Ru(2)	2.7733(5)	2.7333(8)
Ru(1)–Ru(3)	2.7877(5)	—
Ru(1)–Co(1)	2.7192(7)	2.666(1)
Ru(1)–Co(2)	—	2.569(1)
Ru(1)–N(1)	2.105(3)	2.039(5)
Ru(2)–Ru(3)	2.7570(5)	—
Ru(2)–Co(2)	—	2.676(1)
Ru(2)–N(1)	1.935(3)	1.926(5)
Ru(3)–Co(1)	2.6980(7)	—
Ru(3)–N(1)	2.096(3)	—
Co(1)–Co(2)	—	2.545(1)
Co(1)–N(1)	1.714(3)	1.723(5)
Co(2)–N(1)	—	1.950(5)
Co(1)–Cp*(c) <sup>[a]</sup>	1.66	1.656
Ru(1)–N(1)–Ru(2)	86.6(1)	87.1(2)
Ru(1)–N(1)–Ru(3)	83.1(1)	—
Ru(1)–N(1)–Co(1)	90.2(1)	89.9(2)
Ru(1)–N(1)–Co(2)	—	80.2(2)
Ru(2)–N(1)–Ru(3)	86.2(1)	—
Ru(2)–N(1)–Co(1)	175.0(2)	174.3(2)
Ru(2)–N(1)–Co(2)	—	87.3(2)
Ru(3)–N(1)–Co(1)	89.6(1)	—
Co(1)–N(1)–Co(2)	—	87.5(2)

<sup>[a]</sup> Cp\*(c) denotes the centroid of the  $\text{C}_5\text{Me}_5$  rings.

Cluster **2**,  $[\text{Ru}_3\text{Co}(\mu\text{-H})(\text{CO})_9(\eta^5\text{-C}_5\text{Me}_5)(\mu_4\text{-N})]$ , consists of a tetranuclear metal core exhibiting a butterfly geometry. The  $\text{Cp}^*\text{Co}$  fragment occupies a wing-tip position, and the Ru atoms bear three terminal carbonyl ligands each. The centroid of the  $\eta^5\text{-C}_5\text{Me}_5$  ligand is 1.660 Å from the Co(1)

atom, which is similar to the typical distance in  $\text{Cp}^*\text{Co}$  clusters  $[\text{Co}–\text{Cp}^*_{\text{ave.}} 1.695 \text{ Å}]$ .<sup>[5,30]</sup> The nitrido N(1) is semi-encapsulated within the butterfly and is displaced towards Co(1) at a distance of 1.714(3) Å. The hydride ligand revealed by  $^1\text{H}$  NMR spectroscopy was located by Fourier-difference synthesis and was found to bridge the Ru(1)–Ru(3) hinge. Thus, the bond angles Ru(3)–Ru(1)–C(1)/C(3) and Ru(1)–Ru(3)–C(7)/C(9) are larger (average 107.4°) than the corresponding values along the other wings (average 97.1°). The dihedral angle between the butterfly wings in **2** measures 78.6°.

The molecular structure of  $[\text{Ru}_2\text{Co}(\text{CO})_6(\mu_3\text{-CO})(\eta^5\text{-C}_5\text{Me}_5)(\mu_3\text{-NH})]$  (**3**) is depicted in Figure 2, while key bond lengths and angles are listed in Table 3. Cluster **3** contains a heterometallic  $\text{Ru}_2\text{Co}$  triangular metal core, triply-capped in an asymmetric fashion by a  $\mu_3\text{-NH}$  ligand through the coordination of the nitrogen atom [Ru(1)–N(1) 2.017(4) Å, Ru(2)–N(1) 2.019(5) Å, and Co(1)–N(1) 1.862(4) Å] on one side and a  $\mu_3\text{-CO}$  ligand on the other. The nitrene hydrogen and nitrogen atoms give rise to a triplet ( $\delta = 7.46$ ,  $J_{\text{NH}} = 54.80 \text{ Hz}$ ) and a doublet [ $\delta = 131.4$ ,  $J(^{15}\text{NH}) = 76.95 \text{ Hz}$ ] in the  $^1\text{H}$  and  $^{15}\text{N}$  NMR spectra, respectively. Both signals are downfield shifted compared with those of  $[\text{Ru}_3(\mu\text{-H})_2(\text{CO})_9(\mu_3\text{-NH})]$  [ $^1\text{H}$ :  $\delta = 6.33$  (t,  $J_{\text{NH}} = 55.0 \text{ Hz}$ );  $^{15}\text{N}$ :  $\delta = 82.5$  [d,  $J(^{15}\text{NH}) = 77.5 \text{ Hz}$ ]],<sup>[18]</sup> which suggests that the  $\text{Cp}^*\text{Co}$  moiety is more electron-withdrawing than the isolobal  $\text{Ru}(\text{CO})_3$  group. The  $\mu_3$ -capping ligand C(7)–O(7) is found to be displaced towards Co(1) at a distance of 1.821(6) Å [Co(1)–C(7)], while the Ru(1)–C(7) and Ru(2)–C(7) distances amount to 2.399(6) and 2.402(6) Å, respectively. The isolation of **3** was unexpected, since one of the ruthenium vertices had to be replaced by an isoelectronic  $(\eta^5\text{-C}_5\text{Me}_5)\text{Co}(\text{CO})$  fragment through a “metal-exchange” reaction.<sup>[31]</sup> Such metal-exchange reactions are known, but are not common in cluster chemistry.<sup>[31–33]</sup>

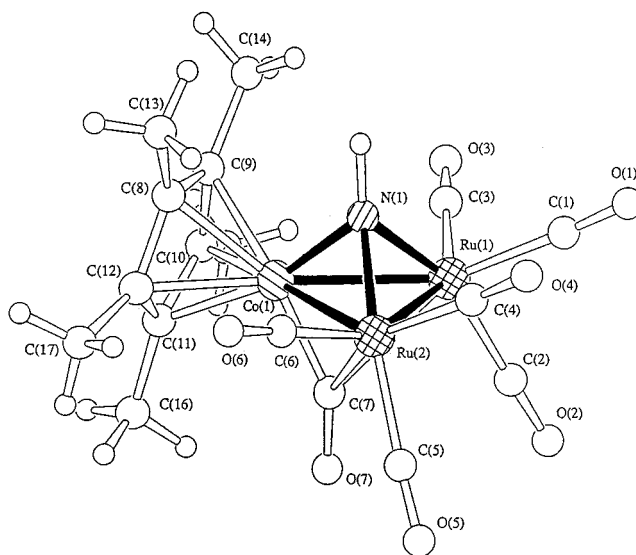


Figure 2. The molecular structure of  $[\text{Ru}_2\text{Co}(\text{CO})_6(\mu_3\text{-CO})(\eta^5\text{-C}_5\text{Me}_5)(\mu_3\text{-NH})]$  (**3**) showing the atom numbering scheme



Table 3. Selected bond lengths [Å] and angles [°] for cluster **3**

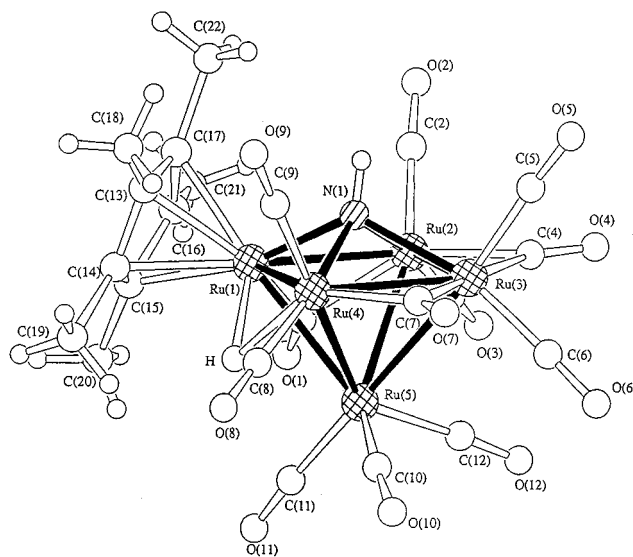
Ru(1)–Ru(2)	2.7093(7)
Ru(1)–Co(1)	2.6009(9)
Ru(1)–N(1)	2.017(4)
Ru(2)–Co(1)	2.6101(8)
Ru(2)–N(1)	2.019(5)
Co(1)–N(1)	1.862(4)
Co(1)–Cp*(c) <sup>[a]</sup>	1.695
N(1)–H	1.07
Ru(2)–Ru(1)–Co(1)	58.84(2)
Ru(1)–Ru(2)–Co(1)	58.51(2)
Ru(1)–Co(1)–Ru(2)	62.65(2)
Ru(1)–N(1)–Ru(2)	84.3(2)
Ru(1)–N(1)–Co(1)	84.1(1)
Ru(2)–N(1)–Co(1)	84.4(2)

<sup>[a]</sup> Cp\*(c) denotes the centroid of the C<sub>5</sub>Me<sub>5</sub> rings.

Besides these heterometallic complexes, a pentaruthenium  $\mu_4$ -nitrene cluster **4** was also isolated from this reaction. Its IR spectrum features vibrational absorptions due to both the terminal and bridging carbonyl ligands. Its <sup>1</sup>H NMR spectrum displays a triplet centred at  $\delta = 6.28$  with a coupling constant of 48.82 Hz, which may be attributed to the NH proton. Resonances at  $\delta = 2.20$  and  $-14.92$  are assigned to the Cp\* and hydride ligands, respectively. The presence of a quadruply-bridging nitrene ligand is evident from the <sup>15</sup>N NMR spectrum, which shows a doublet at  $\delta = 145.4$  [ $J(^{15}\text{NH}) = 68.26$  Hz] relative to liquid NH<sub>3</sub>. Four absorption bands at 330, 345, 405, and 466 nm are seen in the UV/vis spectrum of **4** (Table 1).

Red crystals of **4**, suitable for X-ray diffraction studies, were grown from a saturated solution in CHCl<sub>3</sub>/*n*-hexane at  $-20^\circ\text{C}$ . The molecular structure of **4** is depicted in Figure 3 and the relevant structural parameters are summarized in Table 4. Cluster **4** consists of a square-pyramidal cluster of five ruthenium atoms, with a quadruply-capping NH ligand spanning the square base. A  $\eta^5$ -coordinated C<sub>5</sub>Me<sub>5</sub> ligand, transferred from the external [Cp\*Co(CO)<sub>2</sub>] complex, is coordinated to one basal Ru atom at a distance of 1.856 Å. To the best of our knowledge, [Cp\*Co(CO)<sub>2</sub>] acting as a source of Cp\* in an intermolecular ligand-transfer reaction is very rare in cluster chemistry. A ligand-transfer process of Cp in a comparable ruthenium cluster was observed in [Ru<sub>6</sub>( $\mu_3$ -H)(CO)<sub>12</sub>( $\mu$ -CO)( $\mu_4$ - $\eta^2$ -CO)<sub>2</sub>( $\eta^5$ -C<sub>5</sub>Me<sub>5</sub>)].<sup>[34]</sup> Three of the basal Ru–Ru edges are bridged by carbonyl ligands, while the fourth is bridged by a hydride ligand. The bridging carbonyl and hydride ligands involving the Cp\*-coordinated Ru(1) are found to be slightly disordered among these sites. These two ligands reside in semi-triply-bridging positions, while the other two cap the equatorial sites of the square base. The nonbonding lengths Ru(5)···C(1) and Ru(5)···H are 2.59 Å and 2.33 Å, respectively [cf. Ru(1)–C(1) 2.00(2), Ru(2)–C(1) 2.15(2), Ru(1)–H 1.95, and Ru(4)–H 2.17 Å]. The  $\mu_4$ -NH moiety caps the Ru<sub>4</sub> base in a symmetrical fashion, with an average Ru–N distance of 2.145 Å. The mean deviation from the plane defined by Ru(1), Ru(2), Ru(3), and Ru(4) is 0.0067 Å and the nitrene N atom lies 0.91 Å above this mean plane. Cluster **4** might be viewed as an N-protonated product of a ruthenium  $\mu_5$ -nitrido cluster anion.<sup>[3,35]</sup> For comparison,

in the [Ru<sub>5</sub>(CO)<sub>14</sub>( $\mu_5$ -N)]<sup>−</sup> anion, the nitrido atom resides 0.21(2) Å below the basal plane of the ruthenium atoms and acts as a five-electron donor. By Fourier-difference synthesis using low-angle data, the H atom was found to be located 0.88 Å from the nitrene N atom. In **4**, the  $\mu_4$ -NH moiety is assigned as a four-electron donor, giving a cluster valence electron (CVE) count of 74. This is the same as that for the cluster anion [Ru<sub>5</sub>(CO)<sub>14</sub>( $\mu_5$ -N)]<sup>−</sup>.<sup>[3,35]</sup>

Figure 3. The molecular structure of [Ru<sub>5</sub>( $\mu$ -H)(CO)<sub>9</sub>( $\mu$ -CO)<sub>3</sub>( $\eta^5$ -C<sub>5</sub>Me<sub>5</sub>)( $\mu_4$ -NH)] (**4**) showing the atom numbering schemeTable 4. Selected bond lengths [Å] and angles [°] for cluster **4**

Ru(1)–Ru(2)	2.769(1)
Ru(1)–Ru(4)	2.775(1)
Ru(1)–Ru(5)	2.905(1)
Ru(1)–N(1)	2.098(7)
Ru(2)–Ru(3)	2.726(1)
Ru(2)–Ru(5)	2.868(1)
Ru(2)–N(1)	2.153(8)
Ru(3)–Ru(4)	2.713(1)
Ru(3)–Ru(5)	2.881(1)
Ru(3)–N(1)	2.201(7)
Ru(4)–Ru(5)	2.873(1)
Ru(4)–N(1)	2.128(8)
Ru(1)–Cp*(c) <sup>[a]</sup>	1.856
N(1)–H	0.88
Ru(1)–N(1)–Ru(2)	81.3(3)
Ru(1)–N(1)–Ru(3)	130.3(3)
Ru(1)–N(1)–Ru(4)	82.1(3)
Ru(2)–N(1)–Ru(3)	77.5(2)
Ru(2)–N(1)–Ru(4)	129.0(3)
Ru(3)–N(1)–Ru(4)	77.6(2)

<sup>[a]</sup> Cp\*(c) denotes the centroid of the C<sub>5</sub>Me<sub>5</sub> rings.

In our previous reports,<sup>[13–15]</sup> all the tetraruthenium  $\mu_4$ -NH nitrene ligands have been stabilized by bridging Ru(CO)<sub>4</sub> or  $\mu_4$ - $\eta^2$ -alkyne fragments. However, in the present case, this ligand is stabilized by a quadruply-bridging Ru(CO)<sub>3</sub> moiety. This pseudo-octahedral skeletal framework [Ru<sub>5</sub>( $\mu_4$ -ER)] (R = alkyl or aryl group, etc.) has been seen with phosphorus,<sup>[36–40]</sup> sulfur,<sup>[41–43]</sup> and even carbon.<sup>[44]</sup> This is the first time that a  $\mu_4$ -NH fragment has been observed in this type of structure. The square Ru<sub>4</sub> fragment provides a

model for chemical transformations at the (100) face of metallic ruthenium.<sup>[45,46]</sup> Although ruthenium is a very important catalytic metal, models for the interaction of nitrogen fragments with this (100) array are rare.<sup>[13–15]</sup>

It is believed that cluster **4** is formed by enlargement of the starting triruthenium cluster, with coordination of a Cp\* ligand transferred from the external mononuclear complex. When **1** is heated in THF in the presence of an excess of pentamethylcyclopentadiene and 1,3-cyclohexadiene, **4** is obtained in 4% yield (Scheme 1). In the absence of 1,3-cyclohexadiene, there is no observable reaction under similar conditions, hence the diene must be important in removing a proton from the free Cp\*H ligand. In both synthetic methods {involving [Cp\*Co(CO)<sub>2</sub>] or Cp\*H}, the pentamethylcyclopentadiene is transferred as a Cp\*<sup>−</sup> anion.

The last eluted product is [Ru<sub>6</sub>Co(μ<sub>3</sub>-H)(CO)<sub>8</sub>(μ-CO)<sub>3</sub>(μ<sub>4</sub>-η<sup>2</sup>-CO)(η<sup>5</sup>-C<sub>5</sub>Me<sub>5</sub>)<sub>3</sub>(μ<sub>4</sub>-N)] **5**. Its IR spectrum shows the presence of both terminal and bridging carbonyl ligands (Table 1). The four singlet resonances in its <sup>1</sup>H NMR spectrum, with integrals in the ratio 15:15:15:1, correspond to the three Cp\* ligands and one triply-bridging hydride. With reference to clusters **2–4**, the relatively up-field signal at δ = 1.76 could be assigned to the Cp\* ligand on the Co(1) atom. A downfield singlet at δ = 548.8 is observed in the <sup>15</sup>N NMR spectrum. In the electronic absorption spectrum of **5**, three bands are seen at 360, 390 and 579 nm. X-ray quality crystals of cluster **5** were grown from a CHCl<sub>3</sub>/*n*-hexane solution at −20 °C. A perspective view of the molecular structure is depicted in Figure 4. Selected interatomic distances and angles are listed in Table 5.

The metal framework of **5** consists of a central Ru<sub>4</sub> tetrahedron with an Ru–Ru edge bridged by a Cp\*Co fragment and the other edges bridged by a further two Ru atoms. A structurally related Ru<sub>6</sub> cluster, [Ru<sub>6</sub>(μ<sub>3</sub>-H)(CO)<sub>12</sub>(μ-CO)(μ<sub>4</sub>-η<sup>2</sup>-CO)<sub>2</sub>(η<sup>5</sup>-C<sub>5</sub>Me<sub>5</sub>)],<sup>[34]</sup> has been reported. The difference between cluster **5** and this Ru<sub>6</sub> cluster is that one μ<sub>4</sub>-η<sup>2</sup>-CO of the latter is replaced by a μ<sub>4</sub>-nitrido ligand, which is bound to the Cp\*Co moiety. Therefore, in **5**, a five-electron μ<sub>4</sub>-N and a four-electron μ<sub>4</sub>-η<sup>2</sup>-CO donor ligand are situated in the two butterfly arrays created by the bridging Co and Ru atoms and the faces of the Ru<sub>4</sub> tetrahedron, respectively. The dihedral angles between the wings of the butterflies are 77.2° and 121.2°. The C–O bond length in the μ<sub>4</sub>-η<sup>2</sup>-carbonyl ligand is considerably longer than the terminal C–O bonds [1.25(2) vs. ave. 1.17(1) Å], which may be attributed to electron donation from the C–O π-bond and a significant reduction in bond order due to the d<sub>π</sub>–p<sub>π</sub> bonding of the three Ru atoms. Besides the η<sup>5</sup>-C<sub>5</sub>Me<sub>5</sub> ligand on the Co atom, the other two must be transferred from other [Cp\*Co(CO)<sub>2</sub>] complexes. One is bound to the apical Ru atom of the central tetrahedron, while the other is coordinated to the spiked-edge Ru(6) atom. The interactions between the Cp\*<sup>−</sup> ligands and Co [Co(1)–Cp\*(c) 1.671 Å] are stronger than those involving the Ru atoms [Ru(2)/Ru(6)–Cp\*(c) 1.890 and 1.907 Å]. A positive charge is considered to be localized on the Co atom, whereas the charges associated with the Ru atoms are delocalized throughout the cluster. This is also consistent

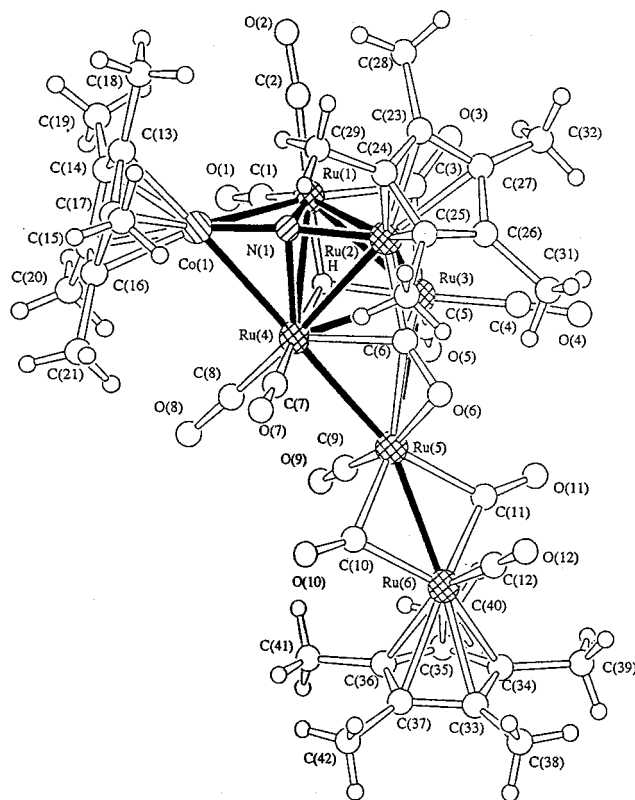


Figure 4. The molecular structure of [Ru<sub>6</sub>Co(μ<sub>3</sub>-H)(CO)<sub>8</sub>(μ-CO)<sub>3</sub>(μ<sub>4</sub>-η<sup>2</sup>-CO)(η<sup>5</sup>-C<sub>5</sub>Me<sub>5</sub>)<sub>3</sub>(μ<sub>4</sub>-N)] (**5**) showing the atom numbering scheme

Table 5. Selected bond lengths [Å] and angles [°] for cluster **5**

Ru(1)–Ru(2)	2.838(2)
Ru(1)–Ru(3)	2.753(2)
Ru(1)–Ru(4)	2.868(2)
Ru(1)–Co(1)	2.709(3)
Ru(1)–N(1)	2.07(1)
Ru(2)–Ru(3)	2.819(2)
Ru(2)–Ru(4)	2.700(3)
Ru(2)–N(1)	1.92(2)
Ru(3)–Ru(4)	2.916(3)
Ru(3)–Ru(5)	2.912(2)
Ru(4)–Ru(5)	2.832(2)
Ru(4)–Co(1)	2.714(3)
Ru(4)–N(1)	2.07(1)
Ru(5)–Ru(6)	2.728(2)
Co(1)–N(1)	1.73(2)
C(6)–O(6)	1.25(2)
Ru(2)–Cp*(c) <sup>[a]</sup>	1.890
Ru(6)–Cp*(c) <sup>[a]</sup>	1.907
Co(1)–Cp*(c) <sup>[a]</sup>	1.671
Ru(2)–Ru(3)–Ru(5)	94.11(6)
Ru(2)–Ru(4)–Ru(5)	98.61(8)
Ru(5)–Ru(4)–Co(1)	170.75(8)
Ru(3)–Ru(5)–Ru(6)	146.94(9)
Ru(4)–Ru(5)–Ru(6)	150.71(8)
Ru(1)–N(1)–Ru(2)	90.7(6)
Ru(1)–N(1)–Ru(4)	87.8(4)
Ru(1)–N(1)–Co(1)	90.5(6)
Ru(2)–N(1)–Ru(4)	85.1(5)
Ru(2)–N(1)–Co(1)	175.5(9)
Ru(4)–N(1)–Co(1)	90.6(7)
Ru(2)–C(6)–O(6)	139(1)

<sup>[a]</sup> Cp\*(c) denotes the centroid of the C<sub>5</sub>Me<sub>5</sub> rings.

with the observation of short Ru(2)–Ru(4) and Ru(5)–Ru(6) bond lengths. A further supporting argument provided by the  $^1\text{H}$  NMR resonances of the relevant  $\text{Cp}^*$  ligands. This  $\text{Ru}_6\text{Co}$  metal skeleton is seldom found in either homo- or heterometallic cluster chemistry. The hydride ligand, which gives rise to a signal at  $\delta = -26.46$  in the  $^1\text{H}$  NMR spectrum, was located by Fourier-difference synthesis and was found to cap beneath the basal plane, Ru(1)–Ru(3)–Ru(4), of the central  $\text{Ru}_4$  tetrahedron. The formation of **4** and **5** is clearly a complex transformation involving the scavenging of additional ruthenium atoms and the incorporation of  $\text{Cp}^*$  ligands from the mononuclear complexes. The overall yields of **4** and **5** are accordingly modest and lower than those of clusters **2** and **3**.

### Conversion between **2** and **3**

#### (a) Reaction of **2** with DBU

The reaction of cluster **2** with 1 equivalent of DBU (1,8-diazabicyclo[5.4.0]undec-7-ene) was monitored by  $^1\text{H}$  NMR spectroscopy. The sterically hindered base DBU is commonly used as a deprotonating agent for metal clusters and a mechanism for this type of reaction has been proposed.<sup>[47]</sup> The hinge-bridged hydride was found to undergo dissociation within a few minutes (Scheme 2). This reaction proved to be irreversible; deprotonated **2** was not converted back to **2** upon addition of a slight excess of  $\text{CF}_3\text{COOH}$ . Instead of re-protonation, the deprotonated cluster **2** underwent degradation to give **3** along with significant decomposition products.

#### (b) Reaction of **2** with $[\text{Cp}^*\text{Co}(\text{CO})_2]$

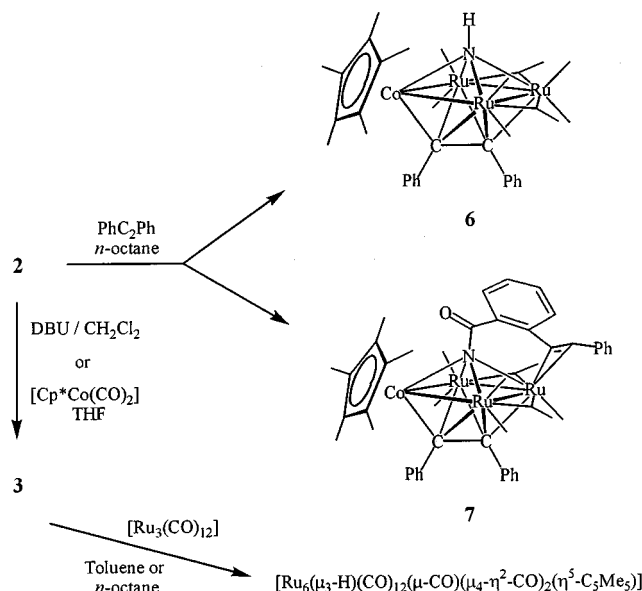
Compound **2** was allowed to react with excess  $[\text{Cp}^*\text{Co}(\text{CO})_2]$  in refluxing THF for 10 h (Scheme 2). After removing the solvent in vacuo, chromatographic separation of the residue gave a moderate yield of cluster **3** as the only isolable product.

#### (c) Reaction of **3** with $[\text{Ru}_3(\text{CO})_{12}]$

In an attempt to convert **3** to **2**, compound **3** was allowed to react with a slight excess of  $[\text{Ru}_3(\text{CO})_{12}]$  in a high boiling point solvent such as toluene or *n*-octane. After refluxing for 4 h, the known  $[\text{Ru}_6(\mu_3\text{-H})(\text{CO})_{12}(\mu\text{-CO})(\mu_4\text{-}\eta^2\text{-CO})_2(\eta^5\text{-C}_5\text{Me}_5)]$ <sup>[34]</sup> cluster had been produced in 10% yield, accompanied by starting material **3** and decomposition products (see Scheme 2). Cluster **3** was thus largely unreactive under these conditions and no significant change was observed over a period of 12 h. A high energy barrier preventing the desired reaction probably led instead to the degradation of the  $[\text{Ru}_3(\text{CO})_{12}]$  cluster to give mononuclear fragments, thereby accounting for the observed reaction.

### Thermolysis of **2** with $\text{PhC}_2\text{Ph}$

It has been shown previously that protonation of  $[\text{PPN}][\text{Ru}_4(\text{CO})_{12}(\mu_4\text{-N})]$  in the presence of diphenylacetylene gives a  $\mu_4\text{-NH}$  containing species,  $[\text{Ru}_4(\text{CO})_9(\mu\text{-CO})_2(\mu_4\text{-NH})(\mu_4\text{-}\eta^2\text{-PhC}_2\text{Ph})]$ .<sup>[48]</sup> Moreover, treatment of



Scheme 2. Deprotonation of cluster **2** in  $\text{CH}_2\text{Cl}_2$  with DBU afforded only **3**; treatment of **2** with  $[\text{Cp}^*\text{Co}(\text{CO})_2]$  in refluxing THF also gave **3**; thermolysis of **2** in *n*-octane with a slight excess of  $\text{PhC}_2\text{Ph}$  resulted in the isolation of  $[\text{Ru}_3\text{Co}(\text{CO})_6(\mu\text{-CO})_2(\eta^5\text{-C}_5\text{Me}_5)(\mu_4\text{-NH})(\mu_4\text{-}\eta^2\text{-PhC}_2\text{Ph})]$  (**6**) and  $[\text{Ru}_3\text{Co}(\text{CO})_5(\mu\text{-CO})_2(\eta^5\text{-C}_5\text{Me}_5)\{\mu_4\text{-}\eta^3\text{-NC}(\text{O})\text{C}_2(\text{C}_4\text{H}_4)\text{CHCH}(\text{Ph})\}(\mu_4\text{-}\eta^2\text{-PhC}_2\text{Ph})]$  (**7**) in yields of 18% and 6%, respectively; attempted preparation of cluster **2** from cluster **3** with  $[\text{Ru}_3(\text{CO})_{12}]$  led only to the known  $[\text{Ru}_6(\mu_3\text{-H})(\text{CO})_{12}(\mu\text{-CO})(\mu_4\text{-}\eta^2\text{-CO})_2(\eta^5\text{-C}_5\text{Me}_5)]$ <sup>[34]</sup>

$[\text{Ru}_3(\mu\text{-H})_2(\text{CO})_9(\mu_3\text{-NPh})]$  with diphenylacetylene was found to afford a  $\mu_4\text{-nitrene}$  cluster  $[\text{Ru}_4(\text{CO})_9(\mu\text{-CO})_2(\mu_4\text{-NPh})(\mu_4\text{-}\eta^2\text{-PhC}_2\text{Ph})]$ .<sup>[49]</sup> Therefore, alkynes are thought to have an important structural stabilizing effect, facilitating the formation and isolation of  $\mu_4\text{-nitrene}$ -containing clusters. Cluster **2**, a molecule with a  $\mu_4\text{-nitrido}$  group coordinated between the wings of an  $\text{Ru}_3\text{Co}$  butterfly, was thus submitted to skeletal expansion reactions with diphenylacetylene in *n*-octane, which led to the incorporation of a two-carbon fragment into the cluster framework (Scheme 2). Separation by preparative TLC gave two major products,  $[\text{Ru}_3\text{Co}(\text{CO})_6(\mu\text{-CO})_2(\eta^5\text{-C}_5\text{Me}_5)(\mu_4\text{-NH})(\mu_4\text{-}\eta^2\text{-PhC}_2\text{Ph})]$  (**6**) and  $[\text{Ru}_3\text{Co}(\text{CO})_5(\mu\text{-CO})_2(\eta^5\text{-C}_5\text{Me}_5)\{\mu_4\text{-}\eta^3\text{-NC}(\text{O})\text{C}_2(\text{C}_4\text{H}_4)\text{CHCH}(\text{Ph})\}(\mu_4\text{-}\eta^2\text{-PhC}_2\text{Ph})]$  (**7**) in yields of 18% and 6%, respectively. Their spectroscopic data are presented in Table 1. The IR spectra show the presence of both terminal and bridging carbonyl ligands. In the UV/vis spectrum of **6**, absorption bands are seen at 296, 330, 420, and 505 nm. The  $^1\text{H}$  NMR signals due to the organic moieties of **6** and **7** are fully consistent with the proposed structures. Detailed assignments of the protons of the diphenylacetylene ligands were made with the aid of a 2D HH-COSY experiment (see Table 1). In both **6** and **7**, the protons of the phenyl group on the acetylenic carbon  $\sigma$ -bonded to the Ru atom are seen to have similar chemical shifts as those in  $[\text{Ru}_4(\text{CO})_9(\mu\text{-CO})_2(\mu_4\text{-NH})(\mu_4\text{-}\eta^2\text{-PhC}_2\text{Ph})]$ .<sup>[48]</sup> The signals of the protons of the other phenyl group are subject to a downfield shift due to the effect of the  $\text{Cp}^*\text{Co}$  moiety. The resonances of the protons of these two phenyl groups in both **6** and **7** can be easily assigned with the aid of a 2D HH-COSY experiment. The five protons of the phenyl



group on the acetylenic carbon  $\sigma$ -bonded to Ru in **7** have a significantly different environment. This may be due to some extent to the restriction of rotation in this phenyl ring. The  $^{15}\text{N}$  NMR spectrum of the  $^{15}\text{N}$ -enriched sample of **6** features a doublet at  $\delta = 70.2$  [ $J(^{15}\text{N}\text{H}) = 69.26$  Hz]. The  $^{15}\text{N}$  NMR study of **7** was hindered due to the low yield of this cluster. Nevertheless, the structures of both complexes have been established by X-ray crystallographic studies.

Brown crystals of clusters **6** and **7**, suitable for X-ray diffraction studies, were grown from saturated  $\text{CH}_2\text{Cl}_2/n$ -hexane solutions at  $-20^\circ\text{C}$ . The molecular structures of **6** and **7** are shown in Figure 5 and Figure 6, respectively, and relevant structural parameters are listed in Table 6. The molecular geometries of clusters **6** and **7** are similar in that the three Ru atoms and one Co atom are arranged in a slightly twisted square base. One face of the square is capped by a  $\mu_4$ -nitrene ligand, while the other is spanned by a quadruply-bridging  $\text{PhC}_2\text{Ph}$  ligand. Species analogous to **6**, with  $\text{Ru}(\text{CO})_3$  in place of the  $\text{Cp}^*\text{Co}$  moiety, have previously been obtained in this laboratory by the reaction of  $\text{PhC}_2\text{R}$  ( $\text{R} = \text{H}, \text{Ph}$ ) with the triruthenium methoxynitrido cluster  $[\text{Ru}_3(\text{CO})_9(\mu_3\text{-CO})(\mu_3\text{-NOMe})]$ .<sup>[13,14]</sup> The  $\text{Cp}^*$  ligands are coordinated to the Co atoms at distances of 1.687 and 1.722 Å in **6** and **7**, respectively. The quadruply-bridging diphenylacetylene ligands in **6** and **7** are bound to the metal square through  $\text{C}(19)\text{--}\text{C}(20)$ , with  $\sigma$  interactions to Ru(2) and Co(1) and longer  $\eta^2$  interactions to Ru(1) and Ru(3). The cluster may also be viewed as a pentagonal bipyramid, the basal plane being defined by Ru(2), C(20), C(19), Co(1), and N(1). The mean deviations from the plane defined by the four metal atoms are 0.200 Å in **6** and 0.198 Å in **7**. In both cases, it is the Co(1) atoms that show the greatest deviations from these mean planes, by 0.365 Å in **6** and 0.380 Å in **7**. To the best of our knowledge, these compounds represent the first examples of the coordination of  $\mu_4$ -nitrene fragments to a square  $\text{Ru}_3\text{Co}$  metal cluster. The nitrene N atoms asymmetrically cap the square bases, being tilted towards Co(1). The nitrene N atom lies above the basal plane, with a distance to the mean plane of 1.019 Å and 1.102 Å in clusters **6** and **7**, respectively. In cluster **6**, the hydrogen atom was located by Fourier-difference synthesis using low-angle data at 0.75 Å from the  $\mu_4$ -NH nitrogen atom. A novel coupling reaction is observed in **7**, which involves a carbonyl group, an *ortho*-carbon of a Ph group of the  $\text{PhC}_2\text{Ph}$  ligand, and the  $\mu_4$ -N atom. The activated acetylenic ligand is also found to be coordinated to Ru(2). The carbonyl group coupled between the Ph group and the  $\mu_4$ -N ligand has a C–O bond length of 1.22(1) Å, which is typical for a ketone C=O group. The C(39)–C(40) bond length is significantly lengthened to 1.41(1) Å upon coordination to an Ru centre as the alkyne is reduced to a *trans* alkene.

If the  $\mu_4$ -nitrene and quadruply-bridging diphenylacetylene groups are both assigned as being four-electron donors, the electron count for these metal clusters is 62, which is two electrons less than the expected electron count (64) for a square-planar transition metal cluster.<sup>[50]</sup> Within the formalism of the 18-electron rule, the 62-electron square

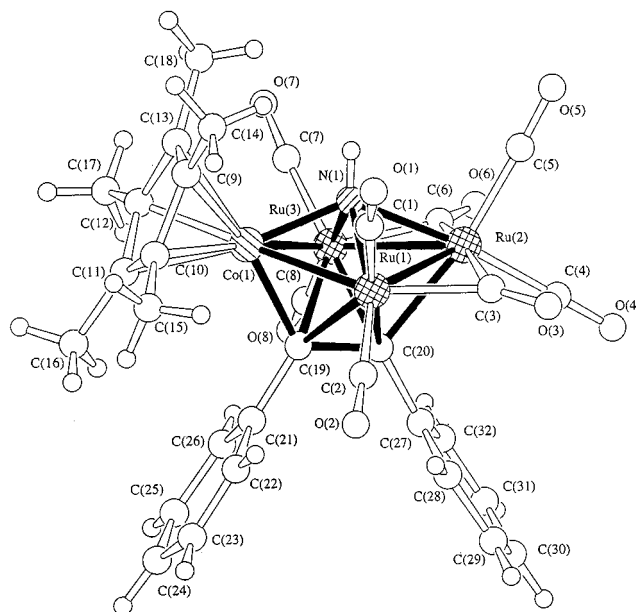


Figure 5. The molecular structure of  $[\text{Ru}_3\text{Co}(\text{CO})_6(\mu\text{-CO})_2(\eta^5\text{-C}_5\text{Me}_5)(\mu_4\text{-NH})(\mu_4\text{-}\eta^2\text{-PhC}_2\text{Ph})]$  (**6**) showing the atom numbering scheme

clusters **6** and **7** are electronically unsaturated, and a 2 electron-3 centre bond has been proposed as being delocalized between the two 17-electron centres and one 16-electron centre bridged by two  $\mu\text{-CO}$  groups. Clusters **6** and **7** can be described as pentagonal-bipyramidal structures if the N and C atoms in both the  $\mu_4$ -NH and the  $\text{PhC}_2\text{Ph}$  units are also considered as skeletal atoms. The electron count for the cluster in such a consideration is 70, conforming to the  $14n + 4m + 2$  rule,<sup>[50]</sup> where  $n$  represents the number of transition metal atoms and  $m$  denotes the number of main group atoms. To further understand the electronic structure of cluster **6**, we carried out molecular orbital calculations on the model cluster  $[\text{Ru}_3\text{Co}(\text{CO})_6(\mu\text{-CO})_2(\eta^5\text{-C}_5\text{H}_5)(\mu_4\text{-NH})(\mu_4\text{-}\eta^2\text{-HC}_2\text{H})]$ .<sup>[51]</sup> The NBO analysis<sup>[52]</sup> shows that the Wiberg bond orders<sup>[53]</sup> of the metal–metal bonds are all appreciably positive (0.14 for Co–Ru, 0.07 for Ru–Ru), indicating the existence of metal–metal bonding. Lesser bond orders for the Ru–Ru bonds are due to of the bridging carbonyls in these bonds. The bond orders for Ru–N and Ru–C ( $\text{HC}_2\text{H}$ ) are 0.20 and 0.30, respectively. Those for Co–N and Co–C ( $\text{HC}_2\text{H}$ ) are 0.45 and 0.60, respectively, making them greater than those of the corresponding Ru–N and Ru–C bonds. These results suggest that the interactions between the metal and the bridging main group atoms are crucial with regard to the stabilities of the clusters. Figure 7 shows spatial plots<sup>[54]</sup> of the highest occupied [Figure 7(a)] and the lowest unoccupied [Figure 7(b)] molecular orbitals. The HOMO is mainly localized on the Ru centres, with a slight Co(d)–Ru(d) antibonding interaction. However, the LUMO is mainly localized on the CpCo fragment, again with a slight Co(d)–Ru(d) antibonding interaction. In the LUMO, the antibonding character between Co and the Cp ligand is also noticeable.

In order to investigate this new class of square-planar  $\mu_4$ -nitrene clusters in detail, molecular orbital calculations



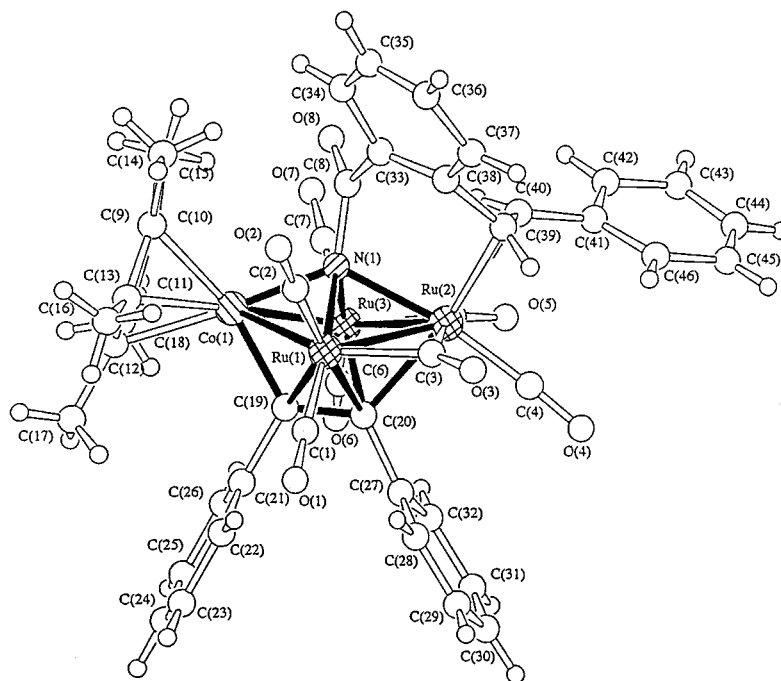


Figure 6. The molecular structure of  $[\text{Ru}_3\text{Co}(\text{CO})_5(\mu\text{-CO})_2(\eta^5\text{-C}_5\text{Me}_5)\{\mu_4\text{-}\eta^3\text{-NC(O)C}_2(\text{C}_4\text{H}_4)\text{CHCH(Ph)}\}(\mu_4\text{-}\eta^2\text{-PhC}_2\text{Ph})]$  (**7**) showing the atom numbering scheme

were also performed on the analogous tetraruthenium  $[\text{Ru}_4(\text{CO})_9(\mu\text{-CO})_2(\mu_4\text{-NOMe})(\mu_4\text{-}\eta^2\text{-PhC}_2\text{Ph})]$  cluster.<sup>[13]</sup> The electron count of this metal cluster is also thought to be 62, which is two electrons less than expected.<sup>[50]</sup> Therefore, a delocalized picture should better describe the electronic structure of the cluster. If the N and C atoms in both the  $\mu_4\text{-NOMe}$  and  $\text{PhC}_2\text{Ph}$  units are also considered as skeletal atoms, the cluster can actually be described as pentagonal-bipyramidal. In this case, the total electron count is 70, again conforming to the  $14n + 4m + 2$  rule.<sup>[50]</sup> In other words, the cluster obeys Wade's  $n + 1$  rule.<sup>[55]</sup> We have also carried out molecular orbital calculations on the model cluster  $[\text{Ru}_4(\text{CO})_9(\mu\text{-CO})_2(\mu_4\text{-NOH})(\mu_4\text{-}\eta^2\text{-HC}_2\text{H})]$ .<sup>[56]</sup> The NBO analysis<sup>[52]</sup> shows that the Wiberg bond orders<sup>[53]</sup> of the four Ru–Ru bonds are all appreciably positive (ca. 0.1), indicating the existence of metal–metal bonding. The corresponding bond orders for Ru–N, Ru–C ( $\text{HC}_2\text{H}$ ), and Ru–CO (bridging) range from 0.15 to 0.55. These results suggest that the metal–ligand interactions are crucial with regard to the stability of the cluster. Figure 8 shows spatial plots<sup>[54]</sup> of the highest occupied molecular orbital (HOMO) [Figure 8(a)] and the lowest unoccupied molecular orbital (LUMO) [Figure 8(b)]. Both the HOMO and LUMO contain the metal(d)–metal(d) antibonding interaction. On careful examination of these orbitals, one can see that the HOMO can be considered as the antibonding combination among the so-called “ $t_{2g}$ ”-like orbitals derived from the relevant metal fragments. These “ $t_{2g}$ ”-like orbitals are approximately nonbonding with respect to the coordinated ligands. However, the LUMO can be described as the skeletal antibonding molecular orbital. The corresponding fragment orbitals in the LUMO involve more metal–ligand antibonding character.

The electronic structures of **6** and  $[\text{Ru}_4(\text{CO})_9(\mu\text{-CO})_2(\mu_4\text{-NOMe})(\mu_4\text{-}\eta^2\text{-PhC}_2\text{Ph})]$  show that both are unsaturated square-planar clusters, which may account for the observed NMR anisotropy. Diamagnetic effects had previously been observed in the  $^1\text{H}$  and  $^{15}\text{N}$  chemical shifts of the  $\mu_4\text{-NH}$  groups in **6** and  $[\text{Ru}_4(\text{CO})_9(\mu\text{-CO})_2(\mu_4\text{-NH})(\mu_4\text{-}\eta^2\text{-PhC}_2\text{Ph})]$ .<sup>[13,48]</sup> In comparison with the electron-precise cluster **4**, the chemical shifts of **6** and the tetraruthenium  $\mu_4\text{-NH}$  clusters appear further upfield. The  $^1\text{H}$  chemical shift of the  $\mu_4\text{-NH}$  proton in the saturated compound **4** is  $\delta = 6.28$ , whereas for the unsaturated compound **6** and the  $\text{Ru}_4$  analogue, the corresponding shifts are  $\delta = 2.76$  and 1.87, respectively. In fact, the  $^1\text{H}$  NMR resonance of the  $\mu_4\text{-NH}$  moiety is a sensitive probe for delineating the bonding type in all these new clusters. The  $^{15}\text{N}$  chemical shifts of the  $\mu_4\text{-NH}$  groups follow the same trend; thus, for the unsaturated clusters **6** and  $[\text{Ru}_4(\text{CO})_9(\mu\text{-CO})_2(\mu_4\text{-NH})(\mu_4\text{-}\eta^2\text{-PhC}_2\text{Ph})]$ <sup>[13,48]</sup> the NH signals are seen at  $\delta = 70.2$  and 47.6, while for the saturated **4** it is found at  $\delta = 145.4$ . The nature of the NMR anisotropy leads to a weaker effective magnetic field above the centre of the  $\text{Ru}_3\text{Co}/\text{Ru}_4$  ring in the unsaturated compounds.<sup>[57]</sup>

Migration of a hydride ligand to the nitrido atom is an essential step in the formation of **6** and **7**. This probably involves a hydride shift to give structure **I**, as shown below.

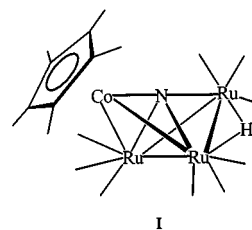
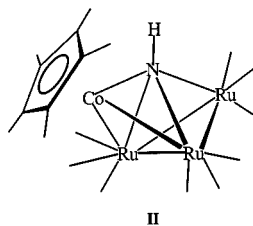


Table 6. Selected bond lengths [Å] and angles [°] for clusters **6** and **7**

	<b>6</b>	<b>7</b>
Ru(1)–Ru(2)	2.694(1)	2.697(1)
Ru(1)–Co(1)	2.631(2)	2.631(2)
Ru(1)–N(1)	2.176(10)	2.175(8)
Ru(1)–C(19)	2.40(1)	2.366(10)
Ru(1)–C(20)	2.33(1)	2.276(9)
Ru(2)–Ru(3)	2.681(1)	2.703(1)
Ru(2)–N(1)	2.147(10)	2.195(8)
Ru(2)–C(20)	2.23(1)	2.191(10)
Ru(2)–C(39)	—	2.22(1)
Ru(2)–C(40)	—	2.29(1)
Ru(3)–Co(1)	2.634(2)	2.613(2)
Ru(3)–N(1)	2.13(1)	2.180(8)
Ru(3)–C(19)	2.41(1)	2.31(1)
Ru(3)–C(20)	2.328(10)	2.305(9)
Co(1)–N(1)	1.949(10)	2.016(8)
Co(1)–C(19)	1.97(1)	1.970(10)
C(8)–O(8)	1.15(2) [carbonyl]	1.22(1)
N(1)–C(8)	—	1.43(1)
C(8)–C(33)	—	1.50(1)
C(19)–C(20)	1.44(2)	1.43(1)
Co(1)–Cp*(c) <sup>[a]</sup>	1.687	1.722
N(1)–H	0.75	—
Ru(1)–N(1)–Ru(2)	77.1(3)	76.2(2)
Ru(1)–N(1)–Ru(3)	114.7(4)	110.4(3)
Ru(1)–N(1)–Co(1)	79.1(3)	77.7(3)
Ru(1)–N(1)–C(8)	—	128.6(7)
Ru(2)–N(1)–Ru(3)	77.5(3)	76.3(2)
Ru(2)–N(1)–Co(1)	136.4(5)	132.8(4)
Ru(2)–N(1)–C(8)	—	108.1(7)
Ru(3)–N(1)–Co(1)	80.2(3)	76.9(3)
Ru(3)–N(1)–C(8)	—	120.5(7)
Co(1)–N(1)–C(8)	—	118.9(7)
O(8)–C(8)–N(1)	—	122(1)
O(8)–C(8)–C(33)	—	119(1)
N(1)–C(8)–C(33)	—	118.4(10)
Ru(2)–C(39)–C(40)	—	74.3(6)
C(38)–C(39)–C(40)	—	120.5(9)
Ru(2)–C(40)–C(39)	—	69.3(6)
C(39)–C(40)–C(41)	—	125.6(9)

<sup>[a]</sup> Cp\*(c) denotes the centroid of the C<sub>5</sub>Me<sub>5</sub> rings.

This type of skeleton has been structurally established in another system.<sup>[58]</sup> The hydrogen atom shows a preference for the ruthenium sites as opposed to those involving the Co(1) atom.<sup>[59]</sup> The hydride ligand eventually migrates to the nitrogen atom to give structure **II** in the case of **6**.



Conceptually, the addition of an acetylene group to **II** can easily be described as an insertion of the C≡C unit into the hinge M–M bond of the cluster. Concomitant unfolding of the wings of the butterfly allows stabilization of the acetylene through direct interaction with all four metal centres. A further coupling of a carbonyl ligand and a PhC<sub>2</sub>Ph ligand to the nitrene N atom is observed in cluster **7**. The metal-bonded H atom and the H on the *ortho*-car-

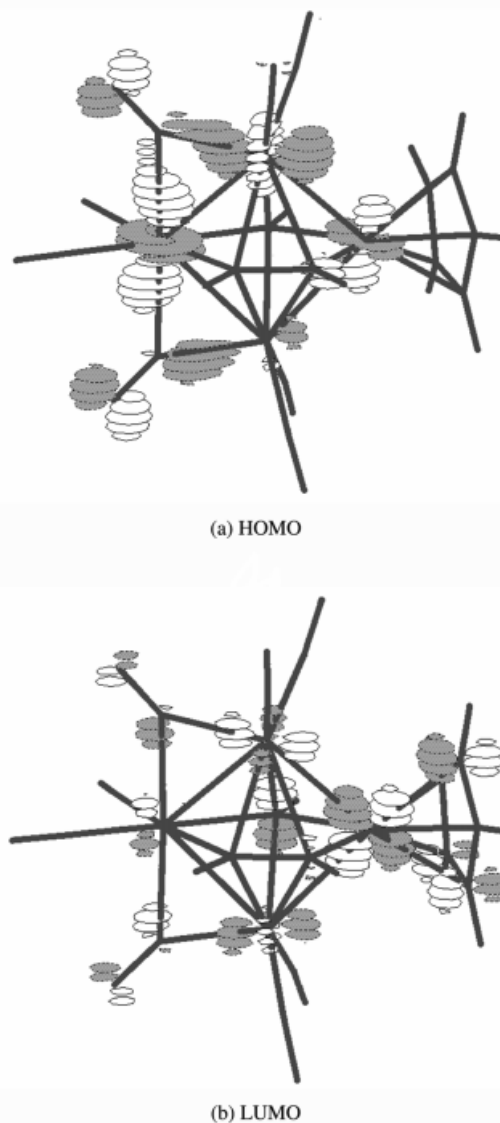


Figure 7. Spatial plots of the highest occupied (a) and the lowest unoccupied (b) molecular orbitals for [Ru<sub>3</sub>Co(CO)<sub>6</sub>(μ-CO)<sub>2</sub>(η<sup>5</sup>-C<sub>5</sub>H<sub>5</sub>)(μ<sub>4</sub>-NH)(μ<sub>4</sub>-η<sup>2</sup>-HC<sub>2</sub>H)]

bon atom are transferred to the acetylenic carbons in a *trans* configuration and give rise to doublet resonances at δ = 5.75 and 2.72 with a mutual coupling of 12.26 Hz. Heating of **6** with PhC<sub>2</sub>Ph under similar reaction conditions does not give any observable amount of **7**, indicating that the H atom is not easily detached from the nitrene N atom. The shortcomings of bridging or capping main group atoms as cluster stabilizing entities have long been established.<sup>[49,60–70]</sup> However, in the present case, the main-group N-atom is shown to be valuable not only for its influence on incoming ligands, but also for its capacity to participate in skeletal rearrangements while maintaining cluster nuclearity.

#### Reaction of [Ru<sub>3</sub>Co(CO)<sub>12</sub>(μ<sub>4</sub>-N)] with [Cp\*Co(CO)<sub>2</sub>]

In order to prepare some Co-rich mixed-metal clusters by a stepwise reaction, the cluster [Ru<sub>3</sub>Co(CO)<sub>12</sub>(μ<sub>4</sub>-N)]<sup>[1]</sup>

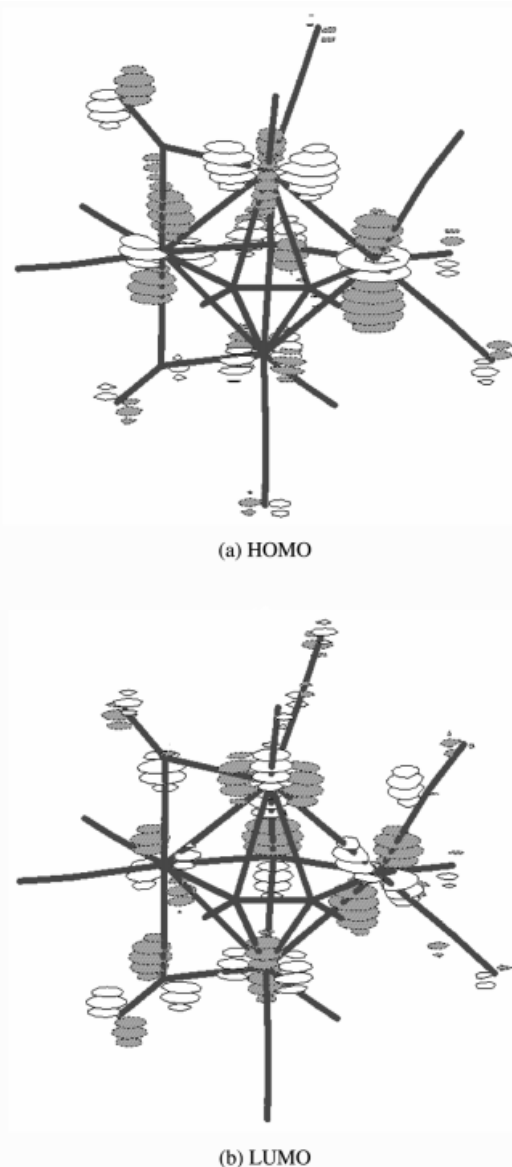
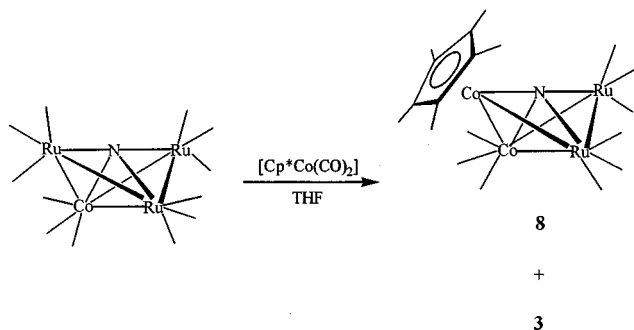


Figure 8. Spatial plots of the highest occupied (a) and the lowest unoccupied (b) molecular orbitals for  $[\text{Ru}_4(\text{CO})_9(\mu\text{-CO})_2(\mu_4\text{-NOH})(\mu_4\text{-}\eta^2\text{-HC}_2\text{H})]$

was allowed to react with  $[\text{Cp}^*\text{Co}(\text{CO})_2]$  in refluxing THF for 4 h (Scheme 3). Dark-brown crystals of  $[\text{Ru}_2\text{Co}_2(\text{CO})_9(\eta^5\text{-C}_5\text{Me}_5)(\mu_4\text{-N})]$  (**8**) were obtained in high yield, accompanied by some **3**. Cluster **8** was fully characterized by conventional spectroscopic techniques and elemental analysis (Table 1). The  $^1\text{H}$  and  $^{15}\text{N}$  NMR spectra of **8** feature singlet resonances at  $\delta = 1.89$  and  $\delta = 524.7$ , respectively. The electronic absorption spectrum of cluster **8** is virtually identical to that of **2**, consisting of four bands at 315, 360, 435, and 520 nm. A single-crystal X-ray analysis was carried out; the structure of **8** is depicted in Figure 9, while selected bond parameters are collected in Table 2.

The two ruthenium and two cobalt atoms of cluster **8** define a butterfly metal core, with a nitrogen atom bridging the wing-tip positions of the cluster. The  $\text{Cp}^*$  ligand is coordinated to the wing-tip Co atom at a distance of 1.656 Å.



Scheme 3. Treatment of  $[\text{Ru}_3\text{Co}(\text{CO})_{12}(\mu_4\text{-N})]$  with 2 equiv. of  $[\text{Cp}^*\text{Co}(\text{CO})_2]$  in refluxing THF resulted in the formation of  $[\text{Ru}_2\text{Co}_2(\text{CO})_9(\eta^5\text{-C}_5\text{Me}_5)(\mu_4\text{-N})]$  (**8**) and cluster **3** in yields of 32% and 41%, respectively

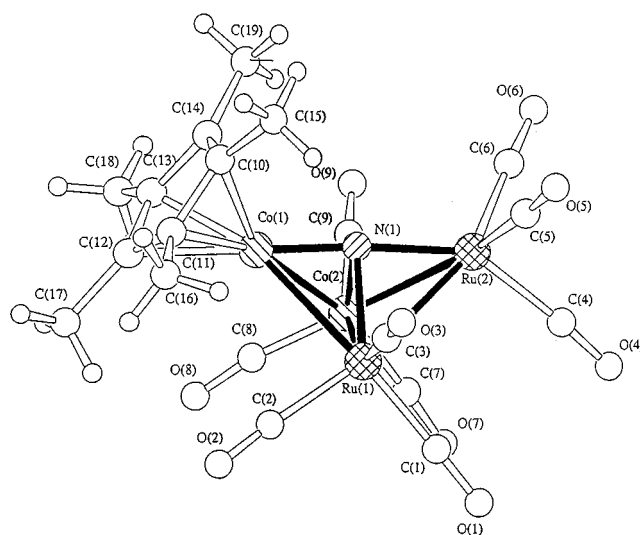
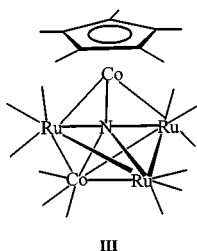


Figure 9. The molecular structure of  $[\text{Ru}_2\text{Co}_2(\text{CO})_9(\eta^5\text{-C}_5\text{Me}_5)(\mu_4\text{-N})]$  (**8**) showing the atom numbering scheme

The same butterfly core was also observed in cluster **2**. Thus, the structure of **8** is related to that of **2**, with a  $\text{Co}(\text{CO})_3$  fragment replacing the hinge  $\text{HRu}(\text{CO})_3$  moiety. Thus, the  $\text{Cp}^*\text{Co}$  moiety in molecule **8** occupies a wing-tip position and the other Co atom is placed at a hinge site. The  $\text{Co}(1)\text{--Co}(2)$  bond in **8** [2.545(1) Å] is significantly longer than that in  $[\text{Co}_3(\mu_3\text{-CO})(\eta^5\text{-C}_5\text{Me}_5)_3(\mu_3\text{-NH})]$ .<sup>[5]</sup> The M–N bond lengths involving the wing-tip metals  $[\text{Ru}(2)\text{--N}(1)$  1.926(5) Å and  $\text{Co}(1)\text{--N}(1)$  1.723(5) Å] are shorter than those involving the hinge metal atoms  $[\text{Ru}(1)\text{--N}(1)$  2.039(5) Å and  $\text{Co}(2)\text{--N}(1)$  1.950(5) Å]. The  $\text{Ru}(1)\text{--N}(1)\text{--Co}(2)$  and  $\text{Ru}(2)\text{--N}(1)\text{--Co}(1)$  angles are 80.2(2)° and 174.3(3)°, respectively. The dihedral angle between the butterfly wings in **8** measures 103.39°, which is very different from that in **2** (78.59°). The formation of cluster **8** is believed to result from a metal-exchange<sup>[31,32]</sup> reaction, accomplished by an addition–elimination sequence. The first step should be the incorporation of the  $\text{Cp}^*\text{Co}$  fragment into the “butterfly”  $[\text{Ru}_3\text{Co}(\text{CO})_{12}(\mu_4\text{-N})]$  core to give intermediate III.



Although structure III is an electron-precise species, this kind of wing-tip-bridged butterfly metal skeleton involving a  $\mu_3$ -nitrido ligand is rarely observed. The only other known example occurs in  $[\text{Ru}_6(\text{CO})_{13}(\mu\text{-H})(\mu_3\text{-N})(\mu_3\text{-}\eta^2\text{-PhC}_2\text{Ph})_2]$ .<sup>[13]</sup> Thus, an  $\text{Ru}(\text{CO})_3$  or an  $\text{RuCo}(\text{CO})_5$  fragment is eliminated to give a more favourable metal framework, i.e. butterfly [8] or triangular [3] clusters. The source of the nitrene hydrogen in the formation of cluster 3 is uncertain; it may come from the degradation of solvent molecules or from a trace amount of moisture in the solvent.

### Electrochemistry

The electrochemistry of clusters 1–3, 6, and 8 has been examined in  $\text{CH}_2\text{Cl}_2$  by means of cyclic voltammetry and controlled-potential coulometry, using *n*-tetrabutylammonium hexafluorophosphate (TBAHFP) as the supporting electrolyte. The redox potential values obtained are summarized in Table 7; for comparison, those of compounds  $[\text{Ru}_4(\text{CO})_9(\mu\text{-CO})_2(\mu_4\text{-NOMe})(\mu_4\text{-}\eta^2\text{-PhC}_2\text{Ph})]$  (9),  $[\text{Ru}_4(\text{CO})_9(\mu\text{-CO})_2(\mu_4\text{-NH})(\mu_4\text{-}\eta^2\text{-PhC}_2\text{Ph})]$  (10), and  $[\text{Ru}_4(\text{CO})_9(\mu\text{-CO})_2\{\mu_4\text{-NC}(\text{O})\text{OMe}\}(\mu_4\text{-}\eta^2\text{-PhC}_2\text{Ph})]$  (11) are also listed.<sup>[13]</sup>

Table 7. Electrochemical data for compounds 1–3, 6, 8, and  $[\text{Ru}_4(\text{CO})_9(\mu\text{-CO})_2(\mu_4\text{-NR})(\mu_4\text{-}\eta^2\text{-PhC}_2\text{Ph})]$  [9, R = OMe; 10, R = H, and 11, R =  $\text{C}(\text{O})\text{OMe}$ ]<sup>[13]</sup>

Cluster <sup>[a]</sup>	Oxidation $E_{\text{pa}1}$ (V) <sup>[b]</sup>	Reduction $E_{\text{pc}1}$ (V) <sup>[b]</sup>	$E_{\text{pc}2}$ (V) <sup>[b]</sup>
1	0.83	−2.13	—
2	0.56	(−1.26) <sup>[c]</sup>	—
3	—	−1.68	—
6	(0.79) <sup>[c]</sup>	(−1.36) <sup>[c]</sup>	(−1.71) <sup>[c]</sup>
8	0.55	(−1.13) <sup>[c]</sup>	—
9	—	−1.31	—
10	—	−1.30	—
11	—	−1.29	—

[a] Ca.  $10^{-3}$  M cluster in 0.1 M TBAHFP in dichloromethane at 298 K, the working electrode was made of glassy carbon, the auxiliary electrode and the reference electrode were a platinum wire and  $\text{Ag}/\text{AgNO}_3$ , respectively. Scan rate  $100 \text{ mVs}^{-1}$ . The potentials are referenced to  $\text{Ag}/\text{AgNO}_3$  (0 V) under the same conditions, calibrated with ferrocene. — [b]  $E_{\text{pa}}$  and  $E_{\text{pc}}$  are the anodic and cathodic potentials, respectively. — [c] Values in parentheses are half-wave potential values,  $E_{1/2}$ .

The cluster  $[\text{Ru}_3(\text{CO})_9(\mu_3\text{-CO})(\mu_3\text{-NOMe})]$  exhibits an irreversible cathodic wave ( $E_{\text{pc}}$ ) at  $-1.66 \text{ V}$  vs.  $\text{Ag}/\text{AgNO}_3$ , along with a weak oxidation wave at  $-0.63 \text{ V}$ . The region where the weak oxidation wave appears was initially empty, with the wave appearing after the cathodic wave was traversed. The  $\Delta E_p$  values remained virtually unchanged on varying the scan rates from 50 to  $1000 \text{ mVs}^{-1}$ . For

$[\text{Ru}_3(\text{CO})_9(\mu_3\text{-CO})(\mu_3\text{-NOMe})]$ , an additional irreversible anodic wave is observed at  $E_{\text{pa}} = 1.11 \text{ V}$ . Controlled-potential coulometry at the oxidation step ( $E_w = 1.25 \text{ V}$ ) indicates that this anodic process consumes 1 faraday/mol of  $[\text{Ru}_3(\text{CO})_9(\mu_3\text{-CO})(\mu_3\text{-NOMe})]$ . On the basis of the relative peak currents of the cathodic and anodic waves, the reduction process could be assigned as a one-electron step. The addition of one electron to the cluster  $[\text{Ru}_3(\text{CO})_9(\mu_3\text{-CO})(\mu_3\text{-NOMe})]$  is believed to afford the 49e cluster  $[\text{Ru}_3(\text{CO})_9(\mu_3\text{-CO})(\mu_3\text{-NOMe})]^-$ , which is unstable and loses a CO ligand to give the 47e species  $[\text{Ru}_3(\text{CO})_9(\mu_3\text{-NOMe})]^-$ <sup>[71]</sup> according to an EC mechanism. Cyclic voltammograms of cluster 1 show the same features as those seen for  $[\text{Ru}_3(\text{CO})_9(\mu_3\text{-CO})(\mu_3\text{-NOMe})]$ , with a pair of cathodic and anodic waves at  $E_{\text{pc}} = -2.13 \text{ V}$  and  $E_{\text{pa}} = 0.83 \text{ V}$  vs.  $\text{Ag}/\text{AgNO}_3$ . A small return oxidation wave at  $-0.68 \text{ V}$  is seen for the transient 47e  $[\text{Ru}_3(\mu\text{-H})_2(\text{CO})_8(\mu_3\text{-NOMe})]^-$ , similar to that seen for  $[\text{Ru}_3(\text{CO})_9(\mu_3\text{-CO})(\mu_3\text{-NOMe})]$ . A salient feature of the electrochemical behaviour of the cluster  $[\text{Ru}_3(\mu\text{-H})_2(\text{CO})_9(\mu_3\text{-NOMe})]$  (1) is that this dihydrido derivative of  $[\text{Ru}_3(\text{CO})_9(\mu_3\text{-CO})(\mu_3\text{-NOMe})]$  is both harder to reduce and easier to oxidize than the corresponding  $\mu_3\text{-CO}$ -capped cluster  $[\text{Ru}_3(\text{CO})_9(\mu_3\text{-CO})(\mu_3\text{-NOMe})]$ . The greater difficulty in reducing dihydrido cluster 1 in  $\text{CH}_2\text{Cl}_2$  is shown by the fact that the  $E_{\text{pc}}$  value for the 0/−1 couple is 470 mV more negative than that for  $[\text{Ru}_3(\text{CO})_9(\mu_3\text{-CO})(\mu_3\text{-NOMe})]$ . Likewise, the +1/0 oxidation couple of 1 is less positive than that for  $[\text{Ru}_3(\text{CO})_9(\mu_3\text{-CO})(\mu_3\text{-NOMe})]$  by 280 mV. These data are consistent with the premise that the hydrido ligands effectively function as stronger  $\sigma$ -electron donors and as weaker  $\pi$ -acceptors than  $\mu_3\text{-CO}$  ligands.

Although clusters 2 and 8 are obtained from different reactions, they have similar metal architectures and ligand dispositions, with an Ru atom and a hinge  $\mu\text{-H}$  in 2 being replaced by a Co atom in 8. Both exhibit similar electrochemical behaviour in their cyclic voltammograms. Two electrode processes are evident from their voltammograms: (i) a reversible reduction wave at  $-1.26 \text{ V}$  for 2 and at  $-1.13 \text{ V}$  for 8, and (ii) an irreversible oxidation wave at around 0.55 V. The species with the higher cobalt-content, cluster 8, is easier to reduce to the corresponding monoanionic derivative. Controlled-potential electrolyses at  $E_w = -1.4 \text{ V}$  for 2 and  $-1.3 \text{ V}$  for 8 showed that the reduction processes involve one faraday/mol of cluster molecule. Cyclic voltammetric tests run after exhaustive electrolyses showed that the 0/−1 cathodic steps are chemically reversible. On the other hand, controlled-potential coulometry run at 0.7 V for both 2 and 8 showed that two electrons are removed for each molecule. Cluster 8 was found to decompose further, while cluster 2 was stoichiometrically converted into cluster 3. Analysis of the cyclic voltammetric responses relating to the cathodic peaks of 2 and 8, with scan rates  $\nu$  varying from  $50 \text{ mVs}^{-1}$  to  $1000 \text{ mVs}^{-1}$ , indicated that: (i) the peak current ratio  $i_{\text{pa}}/i_{\text{pc}}$  remains close to unity, (ii) the current function (proportional to  $i_{\text{pc}}/\nu^{1/2}$ ) is essentially constant, and (iii) the peak-to-peak separation is between 80 and 100 mV. This trend in peak-to-peak separation parallels that obtained for ferrocene under the same



experimental conditions. Thus, we can assume that the reduction steps of both **2** and **8** proceed by an essentially reversible electron-transfer process. Upon one-electron addition, no gross structural variation should occur in these Ru–Co mixed-metal nitrido complexes. The irreversible two-electron oxidations in **2** and **8** can be assigned as following ECEC or EEC processes. After controlled-potential electrolysis of cluster **2** at 0.7 V for 180 min, the current had decayed to background levels and the experiment was halted. Two faradays of charge were required for each mol of **2**, which was found to be almost completely converted into cluster **3**. In order to verify this oxidation process chemically, attempts were made to react **2** with  $\text{Ag}[\text{BF}_4]$  and  $[\text{NO}][\text{PF}_6]$ , since the oxidation of **2** occurred at a potential well within the range of these common oxidizing agents. Although vigorous reactions took place when  $\text{Ag}[\text{BF}_4]$  or  $[\text{NO}][\text{PF}_6]$  was added to the cluster in  $\text{CH}_2\text{Cl}_2$ , no cluster **3** could be detected and only decomposition products were obtained. This may possibly be due to  $\text{Ag}^+$  and  $\text{NO}^+$  reacting with the cluster rather than merely oxidizing it.<sup>[71]</sup> A cyclic voltammetric study of compound **3** in  $\text{CH}_2\text{Cl}_2$  revealed an irreversible one-electron reduction at  $-1.68$  V. With a good  $\pi$ -acceptor  $\mu_3$ -CO ligand, cluster **3** was found to be reduced at a similar potential as the cluster  $[\text{Ru}_3(\text{CO})_9(\mu_3\text{-CO})(\mu_3\text{-NOMe})]$ .

The redox behaviour of  $[\text{Ru}_3\text{Co}(\text{CO})_6(\mu\text{-CO})_2(\eta^5\text{-C}_5\text{Me}_5)(\mu_4\text{-NH})(\mu_4\text{-}\eta^2\text{-PhC}_2\text{Ph})]$  (**6**) is shown in Figure 10. It displays one oxidation and two separated reduction processes, all of which are reversible. Controlled-potential coulometry corresponding to the first cathodic step ( $E_w = -1.5$  V) consumes one electron per molecule. Analyses of the cyclic voltammograms exhibited by  $[\text{Ru}_3\text{Co}(\text{CO})_6(\mu\text{-CO})_2(\eta^5\text{-C}_5\text{Me}_5)(\mu_4\text{-NH})(\mu_4\text{-}\eta^2\text{-PhC}_2\text{Ph})]^{1+/0}$  and  $[\text{Ru}_3\text{Co}(\text{CO})_6(\mu\text{-CO})_2(\eta^5\text{-C}_5\text{Me}_5)(\mu_4\text{-NH})(\mu_4\text{-}\eta^2\text{-PhC}_2\text{Ph})]^{1-/2-}$  lead to the same diagnostic results. Thus, the square  $\text{Cp}^*\text{Ru}_3\text{Co}(\mu_4\text{-NH})$  core exhibits remarkably flexible redox behaviour and, within the short timescale of cyclic voltammetry, is able to accommodate both the addition of two electrons and the removal of one electron without significant molecular strain. Among the clusters discussed so far, only **2**, **6**, and **8** exhibit reversible one-electron transfers, and one common feature of these clusters should be noted: all three have strongly  $\pi$ -bonding  $\eta^5\text{-C}_5\text{Me}_5$  ligands. A correlation of this behaviour may be drawn by comparison with the mononuclear analogues such as ferrocene<sup>[72]</sup> and dibenzenechromium,<sup>[73]</sup> which are also reversibly oxidized. Clusters **2**, **6**, and **8** are derived from the chemistry of metallocenes, where the metallic core is “shielded” from destruction by  $\pi$ -ligands. The same conclusion was reached from bonding calculations on cluster **6**. It is expected that reduction of the cluster leads to break-up of the  $\text{CpCo}$  fragment {in the model cluster  $[\text{Ru}_3\text{Co}(\text{CO})_6(\mu\text{-CO})_2(\eta^5\text{-C}_5\text{H}_5)(\mu_4\text{-NH})(\mu_4\text{-}\eta^2\text{-HC}_2\text{H})]$  or dissociation of the Cp ligand [see Figure 7(b)]. In view of the weak Co(d)–Ru(d) antibonding character of the LUMO for **6**, one may expect this to be more reversible. While oxidation is predicted to enhance the Ru–Co interaction, it would also significantly weaken the Ru–CO (bridging) interactions because the HOMO con-

tains appreciable Ru(d) $\rightarrow$ bridging CO( $\pi^*$ ) back-donation [see Figure 7(a)]. The square-planar  $\mu_4$ -nitrene complex **6** is also found to be unsaturated, having 62 CVE's. Electrochemically, it would be expected to take up two electrons to achieve a stable 64-CVE configuration, which is indeed observed; cluster **6** undergoes two sequential, chemically reversible, one-electron additions.

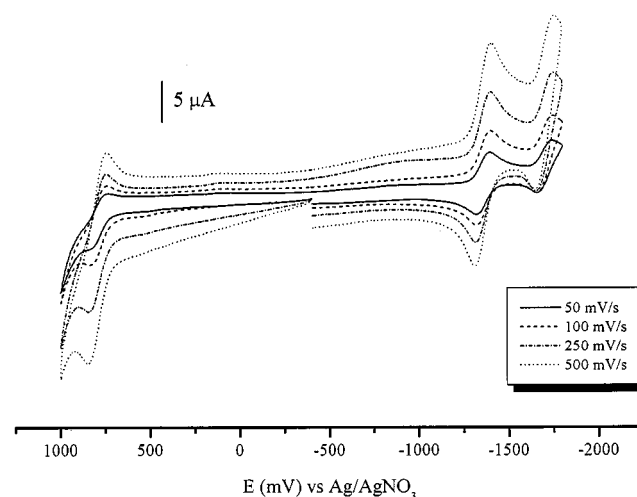


Figure 10. Cyclic voltammogram of **6** in  $\text{CH}_2\text{Cl}_2$  with 0.1 M TBAHFP as supporting electrolyte using glassy carbon working electrode at 298 K; the increasing current arises from scans at 50, 100, 250, and 500 mV/s, respectively; the voltammograms were recorded against an  $\text{Ag}/\text{AgNO}_3$  reference electrode

We also examined the electrochemical behaviour of the clusters  $[\text{Ru}_4(\text{CO})_9(\mu\text{-CO})_2(\mu_4\text{-NR})(\mu_4\text{-}\eta^2\text{-PhC}_2\text{Ph})]$  [**9**, R = OMe; **10**, R = H, and **11**, R = C(O)OMe]. In view of the close similarities in ligation and structure for these three 62-electron bicapped tetraruthenium clusters containing a diphenylacetylene ligand and a  $\mu_4$ -capped nitrene moiety, it is not surprising that they show similar redox characteristics. Clusters **9**, **10**, and **11** exhibit only irreversible reductions within the solvent limits. The value of the cathodic peak potential ( $E_{pc}$ ) is about  $-1.3$  V. Weak oxidation waves are observed at  $-0.99$  V and  $-0.38$  V for **9**, at  $-0.68$  V for **10**, and at  $-0.78$  V for **11** upon scan reversal. Increased scan rates did not lead to any noticeable reversibility of the redox couple. Exhaustive electrolyses on all three clusters **9**, **10**, and **11** at  $E_w = -1.45$  V showed that the cathodic step involves the addition of one electron per molecule. The absence of a re-oxidation wave for this 0/–1 redox couple indicates the existence of a fast chemical follow-up step that extricates the mono-reduced clusters from solution before they can be oxidized back to the neutral clusters. In accordance with the electronic structure of **9** outlined above, we expect reduction of the cluster to destabilize the metal–metal interactions and to lead to fragmentation, while oxidation can be expected to enhance the interaction. With respect to the reduction scan, these results are consistent with the electrochemical behaviour of **9**; however, no oxidation wave is observed within the potential range of the solvent, thus the comment regarding the oxidation scan cannot be verified. Cluster **6** has a similar structure to cluster **10**, except that the  $\text{Cp}^*\text{Co}$  moiety is replaced by an

$\text{Ru}(\text{CO})_3$  moiety. The redox behaviour of **10** has been shown to be different from that of **6**. Apart from enhancing the reversibility of the electrochemical processes, the  $\text{Cp}^*$  Co moiety also makes both reduction and oxidation more feasible within the potential range of  $\text{CH}_2\text{Cl}_2$  as the solvent. The behaviour of heterometallic carbonyl clusters is still uncertain.

### $^{15}\text{N}$ NMR Spectroscopy

$^{15}\text{N}$  NMR spectroscopy is a sensitive and informative tool in characterizing cluster nitridos and nitrenes. In our previous report,<sup>[13]</sup> we presented nitrogen-15 magnetic resonance spectroscopic data for a series of  $\mu_4$ -nitrene [ $\mu_4\text{-NH}$ , NOME, or  $\text{NC}(\text{O})\text{OME}$ ] clusters. A  $\mu_5$ -nitrido atom in a bridged-butterfly metal skeleton was found to exhibit an unusually high-frequency signal ( $\delta = 549.8$ ). In order to investigate the environments of the various nitrogen atoms of the homo- or heterometallic compounds in this study, all the clusters except **7** were examined by  $^{15}\text{N}$  NMR. Table 1 summarizes the  $^{15}\text{N}$  chemical shifts obtained.

The cluster  $[\text{Ru}_3(\text{CO})_9(\mu_3\text{-CO})(\mu_3\text{-NOME})]$ , formed by the reaction of  $[\text{PPN}][\text{Ru}_3(\text{CO})_{10}(\mu\text{-NO})]$  with  $\text{CF}_3\text{SO}_3\text{CH}_3$ , shows a resonance at  $\delta = 287.3$  (reference: liq.  $\text{NH}_3$ ) in its  $^{15}\text{N}$  NMR spectrum when the compound is 90% enriched with  $^{15}\text{N}$ . Hydrogenation of  $[\text{Ru}_3(\text{CO})_9(\mu_3\text{-CO})(\mu_3\text{-NOME})]$  gave cluster  $[\text{Ru}_3(\mu\text{-H})_2(\text{CO})_9(\mu_3\text{-NOME})]$  (**1**), which showed a  $^{15}\text{N}$  chemical shift of  $\delta = 301.0$ .<sup>[29]</sup> Clusters **2** and **3** are the major products of the reaction between **1** and  $[\text{Cp}^*\text{Co}(\text{CO})_2]$ , and exhibit signals at  $\delta = 481.1$  (s) and 131.4 [d,  $J(^{15}\text{NH}) = 76.95$  Hz], respectively. The  $^{15}\text{N}$  NMR signal of **2** lies in the typical range for butterfly species. The  $^{15}\text{N}$  chemical shift of the  $\mu_3\text{-NH}$  N atom of **3** appears 48.9 ppm further downfield compared to that of the corresponding triruthenium  $\mu_3\text{-NH}$  cluster  $[\text{Ru}_3(\mu\text{-H})_2(\text{CO})_9(\mu_3\text{-NH})]$ .<sup>[29]</sup> The  $^{15}\text{N}$  NMR spectrum of  $[\text{Ru}_3(\mu\text{-H})_2(\text{CO})_9(\mu_3\text{-NH})]$  features a doublet at  $\delta = 82.5$  downfield from liquid  $\text{NH}_3$  [ $J(^{15}\text{NH}) = 77.5$  Hz], which is characteristic of a direct NH bond. Cluster **4** can be viewed as the *N*-protonated analogue of  $[\text{Ru}_5(\text{CO})_{14}(\mu_5\text{-N})]^-$ , which gives a  $^{15}\text{N}$  resonance at  $\delta = 464.9$ .<sup>[3]</sup> Cluster **4** gives a doublet at  $\delta = 145.4$  [ $J(^{15}\text{NH}) = 68.26$  Hz], which is significantly upfield (319.5 ppm) from the resonance of  $[\text{Ru}_5(\text{CO})_{14}(\mu_5\text{-N})]^-$ .

The  $^{15}\text{N}$  resonance of **4** is significantly downfield shifted (by 97.8 ppm) compared to that of  $[\text{Ru}_4(\text{CO})_9(\mu\text{-CO})_2(\mu_4\text{-NH})(\mu_4\text{-}\eta^2\text{-PhC}_2\text{Ph})]$ ,<sup>[13]</sup> in which the square-planar  $\text{Ru}_4$  skeleton is stabilized by a quadruply-bridging acetylene ligand to give an electron-precise cluster according to the EAN rule. By comparison with the saturated clusters  $[\text{Ru}_3(\text{CO})_{10}(\mu_2\text{-NH}_2)]$  ( $\delta = -33.5$ ) and  $[\text{Ru}_3(\text{CO})_9(\mu_3\text{-CO})(\mu_3\text{-NH})]$  ( $\delta = 82.5$ ), the resonance of **4** is seen to conform to a smooth trend of increasing magnitude with increasing nuclearity around the hydrogen-bonded nitrogen. Thus, the greater the number of ruthenium atoms bonded to the nitrogen moiety, the more deshielded is the nitrogen resonance. The observed  $J(^{15}\text{NH})$  coupling constants are fully consistent with calculated values based on the  $J(^{14}\text{NH})$  coupling constants [76.86 Hz for **3** and 68.47 Hz for **4**]. Cluster **5** resembles **2**, but with cluster expansion on the  $\text{Ru}_3$  wing face with a triruthenium chain. The further coordination of the triruthenium chain leads to a downfield shift of ca. 68 ppm.  $[\text{Ru}_3\text{Co}(\text{CO})_6(\mu\text{-CO})_2(\eta^5\text{-C}_5\text{Me}_5)(\mu_4\text{-NH})(\mu_4\text{-}\eta^2\text{-PhC}_2\text{Ph})]$  (**6**) is an analogous complex to  $[\text{Ru}_4(\text{CO})_9(\mu\text{-CO})_2(\mu_4\text{-NH})(\mu_4\text{-}\eta^2\text{-PhC}_2\text{Ph})]$ ,<sup>[13]</sup> with an  $\text{Ru}(\text{CO})_3$  moiety being replaced by a  $\text{Co}(\eta^5\text{-C}_5\text{Me}_5)$  group. This exchange leads to a downfield shift in the nitrogen resonance by 22.6 ppm relative to the corresponding  $\text{Ru}_4$  cluster [ $\delta = 47.6$ ,  $J(^{15}\text{NH}) = 70.54$  Hz]. The higher field shifts of the unsaturated  $[\text{Ru}_4(\text{CO})_9(\mu\text{-CO})_2(\mu_4\text{-NH})(\mu_4\text{-}\eta^2\text{-PhC}_2\text{Ph})]$  and **6** relative to the saturated cluster **4** can be attributed to diamagnetic anisotropy effects. In the formation of cluster **6** from **2**, migration of a hydride ligand to the nitrido is involved, hence cluster **6** could be viewed as the “protonation” product of **2** to give the  $\mu_4\text{-NH}$  cluster. The large increase in shielding arising from this direct “protonation” of a butterfly interstitial highlights the large contribution to the deshielding of the interstitial by low-energy circulations of quasi-lone-pair electrons. Similar examples of this have been observed in the protonation of  $[\text{FeRu}_3(\text{CO})_{10}\{\text{P}(\text{OME})_3\}_2]^-$ , both at the hinge and at the nitrogen, to give the  $\mu_4\text{-NH}$  intermediate, where the nitrogen shielding is increased by 231 ppm.<sup>[74]</sup> Protonation of the hinge-protonated carbide  $[\text{HFe}_4\text{C}(\text{CO})_{12}]^{2-}$  to give the  $\mu_4\text{-}\eta^2\text{-CH}$  compound increases the carbon shielding by a correspondingly large amount, i.e. 129 ppm.<sup>[75]</sup> The measurements made in this study on cluster **6** are the first to be

Table 8. Coupling constants of selected  $\mu_3\text{-NH}$  and  $\mu_4\text{-NH}$  ligands

$\mu_3\text{-NH}$ complexes	$J(^{14}\text{NH})$	$J(^{15}\text{NH})$
$[\text{Ru}_2\text{Co}(\text{CO})_6(\mu_3\text{-CO})(\eta^5\text{-C}_5\text{Me}_5)(\mu_3\text{-NH})]$ <b>3</b>	54.80	76.95
$[\text{Ru}_3(\mu\text{-H})_2(\text{CO})_9(\mu_3\text{-NH})]$ <sup>[29]</sup>	—	77.5
$[\text{Ru}_3(\text{CO})_9(\mu_3\text{-CO})(\mu_3\text{-NH})]$ <sup>[74]</sup>	54.0	—
$[\text{FeRu}_2(\text{CO})_9(\mu_3\text{-CO})(\mu_3\text{-NH})]$ <sup>[74]</sup>	54.0	—
$[\text{Fe}_3(\text{CO})_9(\mu_3\text{-CO})(\mu_3\text{-NH})]$ <sup>[77]</sup>	57.0	—
$\mu_4\text{-NH}$ complexes	$J(^{14}\text{NH})$	$J(^{15}\text{NH})$
$[\text{Ru}_5(\mu\text{-H})(\text{CO})_9(\mu\text{-CO})_3(\eta^5\text{-C}_5\text{Me}_5)(\mu_4\text{-NH})]$ <b>4</b>	48.82	68.26
$[\text{Ru}_3\text{Co}(\text{CO})_6(\mu\text{-CO})_2(\eta^5\text{-C}_5\text{Me}_5)(\mu_4\text{-NH})(\mu_4\text{-}\eta^2\text{-PhC}_2\text{Ph})]$ <b>6</b>	49.08	69.26
$[\text{Ru}_4(\text{CO})_9(\mu\text{-CO})_2(\mu_4\text{-NH})(\mu_4\text{-}\eta^2\text{-PhC}_2\text{Ph})]$ <sup>[13]</sup>	50.71	70.54
$[\text{Ru}_4(\text{CO})_9(\mu\text{-CO})_2(\mu_4\text{-NH})(\mu_4\text{-}\eta^2\text{-HC}_2\text{Tol})]$ <sup>[13]</sup>	49.30	70.64

reported for a square  $\text{Ru}_3\text{Co}$  complex having an exclusively quadruply-bridging nitrene ligand. One interesting aspect worth mentioning is that the coupling constants for direct  $^{15}\text{N}$ – $^1\text{H}$  interaction in the  $\mu_4$ –NH moieties are smaller than those for the  $\mu_3$ –NH groups. Table 8 lists coupling constants for the  $\mu_3$ –NH and  $\mu_4$ –NH ligands. The  $^{15}\text{N}$ – $^1\text{H}$  coupling constants can be converted into  $^{14}\text{N}$ – $^1\text{H}$  coupling constants by the equation  $J(^{14}\text{NH}) = -0.713 \times J(^{15}\text{NH})$ , where  $-0.713$  comes from  $\gamma_{14}/\gamma_{15}$ .<sup>[76]</sup> Thus, these characteristic values provide useful information in ascertaining whether the nitrene is bound to three or four metal centres.

Cluster **8** is another butterfly cluster analogous to **2** with a hinge  $\text{HRu}(\text{CO})_3$  fragment replaced by an isolobal  $\text{Co}(\text{CO})_3$  moiety. The  $^{15}\text{N}$  resonance signal is seen at  $\delta = 524.7$  with a downfield shift of 43.6 ppm. In conjunction with the results in our previous report,<sup>[13]</sup> the close relationship between cluster structure and the chemical shift of the cluster nitrogen atom in the  $^{15}\text{N}$  NMR spectra has turned out to be a useful tool for the analysis of the products in this system.

## Conclusion

Triruthenium methoxynitrido carbonyl clusters  $[\text{Ru}_3(\text{CO})_9(\mu_3\text{-CO})(\mu_3\text{-NOMe})]$  and **1** have been extensively studied with regard to deoxygenation to give the coordinated nitrido or nitrene ligands by thermolysis, pyrolysis, or nucleophilic reaction with alkynes. On the basis of various reactivities of the starting clusters, we have demonstrated some new rational high-yielding synthetic routes to the heterometallic tetranuclear nitrido cluster **2**. The formation of this cluster can be simply described as an addition of a mononuclear organometallic complex to the methoxynitrido cluster species with the elimination of two carbonyl ligands and a methanol molecule. The pseudo-octahedral  $\text{Ru}_5\text{N}$  framework arrangement makes cluster **4** a particularly attractive model for surface processes; thus the square  $\text{Ru}_4$  fragment generated constitutes an interesting model for a ruthenium (100) surface. The rather unusual  $\text{Cp}^*$  transfer process has also been observed in this study. Decarbonylation of cluster **2** with an alkyne initiates a hydride migration from a hinge to a nitrido nitrogen atom. This leads to a skeletal rearrangement, where the hinge of the butterfly cluster is ruptured through the insertion of the alkyne ligand. This square  $\text{Ru}_3\text{Co}$  face skeleton presents an opportunity to evaluate nitrene chemistry on a mixed transition metal surface. The incorporation of a  $\text{Cp}^*\text{Co}$  moiety in a  $\mu_4$ –nitrene cluster has been shown to enhance the reversibility of electrochemical processes and make both reduction and oxidation more feasible. Thus, the chemistry of this cluster differs significantly from that observed for homometallic analogues. Both the  $^{15}\text{N}$  NMR and electrochemistry studies of these clusters have provided valuable information regarding the environment of the nitrene/nitrido nitrogen atoms and their redox properties.

## Experimental Section

**General Procedures:** All reactions and manipulations were carried out under argon using standard Schlenk techniques, except for the chromatographic separations. Solvents were purified by standard procedures and distilled prior to use. Unless otherwise stated, all chemicals were purchased commercially and were used as received.  $[\text{Ru}_3(\mu\text{-H})_2(\text{CO})_9(\mu_3\text{-NOMe})]$ ,<sup>[29]</sup>  $[\text{PPN}][^{15}\text{NO}_2]$ ,<sup>[78]</sup> and  $[\text{Cp}^*\text{Co}(\text{CO})_2]$ <sup>[79]</sup> were prepared according to literature methods. – Reactions were monitored by analytical thin-layer chromatography (Merck Kieselgel 60  $\text{F}_{254}$ ) and the products were separated by thin-layer chromatography on plates coated with silica (Merck Kieselgel 60  $\text{GF}_{254}$ ). – Infrared spectra were recorded on a Bio-Rad FTS-7 IR spectrometer with samples in 0.5 mm calcium fluoride solution cells. –  $^1\text{H}$  NMR spectra were recorded on a Bruker DPX300 NMR spectrometer with samples in  $\text{CD}_2\text{Cl}_2$  solution and were referenced to  $\text{SiMe}_4$  ( $\delta = 0$ ). –  $^{15}\text{N}$  NMR spectra were recorded on a Bruker DPX500 NMR spectrometer with samples in  $\text{CDCl}_3$  solution using liq.  $\text{NH}_3$  as a reference. – Positive and negative ionization fast atom bombardment (FAB) mass spectra were recorded on a Finnigan MAT 95 mass spectrometer using *m*-nitrobenzyl alcohol or  $\alpha$ -thioglycerol as matrices. – Electronic absorption spectra were measured at room temperature on a Hewlett–Packard 8453 diode-array UV/vis spectrophotometer with samples in quartz cells with 1 cm path length. – Microanalyses were performed by Butterworth Laboratories, U.K.

**Reaction of  $[\text{Ru}_3(\mu\text{-H})_2(\text{CO})_9(\mu_3\text{-NOMe})]$  (**1**) with  $[\text{Cp}^*\text{Co}(\text{CO})_2]$ :** A solution of  $[\text{Ru}_3(\mu\text{-H})_2(\text{CO})_9(\mu_3\text{-NOMe})]$  (**1**, 100 mg, 0.17 mmol) in THF (50 mL) was heated with 2 equivalents of  $[\text{Cp}^*\text{Co}(\text{CO})_2]$  (83.1 mg, 0.33 mmol) under argon atmosphere. After refluxing for 10 h, the colour of the solution had changed to dark brown. The solvent was then removed under reduced pressure. The residue was redissolved in a small amount of  $\text{CH}_2\text{Cl}_2$  and separated by preparative TLC eluting with *n*-hexane/dichloromethane (6:1, v/v). Four new products were isolated, in the following order of elution: brown  $[\text{Ru}_3\text{Co}(\mu\text{-H})(\text{CO})_9(\eta^5\text{-C}_5\text{Me}_5)(\mu_4\text{-N})]$  (**2**,  $R_f = 0.80$ , 69.8 mg, 0.091 mmol, 55%), trace amounts of starting  $[\text{Ru}_3(\mu\text{-H})_2(\text{CO})_9(\mu_3\text{-NOMe})]$  (**1**,  $R_f = 0.75$ ) and known  $[\text{Ru}_3(\mu\text{-H})(\text{CO})_9(\mu\text{-NH}_2)]$ <sup>[15,29]</sup> ( $R_f = 0.70$ ), purple  $[\text{Ru}_2\text{Co}(\text{CO})_6(\mu_3\text{-CO})(\eta^5\text{-C}_5\text{Me}_5)(\mu_3\text{-NH})]$  (**3**,  $R_f = 0.55$ , 30.3 mg, 0.050 mmol, 20%), red  $[\text{Ru}_5(\mu\text{-H})(\text{CO})_9(\mu\text{-CO})_3(\eta^5\text{-C}_5\text{Me}_5)(\mu_4\text{-NH})]$  (**4**,  $R_f = 0.10$ , 3.0 mg, 0.003 mmol, 3%), and green  $[\text{Ru}_6\text{Co}(\mu_3\text{-H})(\text{CO})_8(\mu\text{-CO})_3(\mu_4\text{-}\eta^2\text{-CO})(\eta^5\text{-C}_5\text{Me}_5)_3(\mu_4\text{-N})]$  (**5**,  $R_f = 0.07$ , 2.4 mg, 0.0017 mmol, 2%). –  $\text{C}_{19}\text{H}_{16}\text{NO}_9\text{CoRu}_3$  (**2**, 764.5): calcd. C 29.84, H 2.09, N 1.83; found C 29.7, H 2.3, N 1.9. –  $\text{C}_{17}\text{H}_{16}\text{NO}_7\text{CoRu}_2$  (**3**, 607.4): calcd. C 33.61, H 2.64, N 2.31; found C 33.7, H 2.4, N 2.4. –  $\text{C}_{22}\text{H}_{17}\text{NO}_{12}\text{Ru}_5$  (**4**, 992.7): calcd. C 26.61, H 1.71, N 1.41; found C 26.8, H 1.8, N 1.6. –  $\text{C}_{42}\text{H}_{46}\text{NO}_{12}\text{CoRu}_6$  (**5**, 1422.2): calcd. C 35.47, H 3.24, N 0.99; found C 35.6, H 3.1, N 1.0.

**Reaction of Complex **1** with Pentamethylcyclopentadiene and 1,3-Cyclohexadiene:** A solution of complex **1** (30 mg, 0.050 mmol) in THF (30 mL) was heated with 1 drop each of pentamethylcyclopentadiene and 1,3-cyclohexadiene under argon atmosphere. The initially yellow solution turned brown upon refluxing. After 10 h, the reaction mixture was concentrated to dryness under reduced pressure. The residue was redissolved in  $\text{CH}_2\text{Cl}_2$  (2 mL) and separated by preparative TLC eluting with *n*-hexane/ $\text{CH}_2\text{Cl}_2$  (2:1, v/v) to afford one red band containing **4** ( $R_f = 0.40$ ) corresponding to a 4% yield (1.2 mg, 0.0012 mmol). The reaction of complex **1** with a drop of pentamethylcyclopentadiene was also attempted in the absence of 1,3-cyclohexadiene under otherwise similar conditions. The refluxing mixture was monitored by IR and spot TLC, but no reac-



tion was observed. About 80% of the starting material was recovered by TLC work-up on preparative silica plates.

**Reaction of Complex 2 with DBU:** Compound **2** (20 mg, 0.026 mmol) was stirred in basified dichloromethane (20 mL) [prepared by the addition of DBU (1,8-diazabicyclo[5.4.0]undec-7-ene) (0.2 mL of 0.13 M solution in CH<sub>2</sub>Cl<sub>2</sub>) to distilled dichloromethane (20 mL)]. The reaction was monitored by spot TLC and <sup>1</sup>H NMR spectroscopy until all the starting material had been consumed (about 10 min). The solvent was then removed under reduced pressure and the residue was chromatographed on silica using *n*-hexane/dichloromethane (6:1, *v/v*) as eluent. The only isolable product was cluster **3** (*R*<sub>f</sub> = 0.55; 3.6 mg, 0.0059 mmol, 15%).

**Reaction of Complex 2 with [Cp\*Co(CO)<sub>2</sub>]:** A solution of cluster **2** (20 mg, 0.026 mmol) and [Cp\*Co(CO)<sub>2</sub>] (9.8 mg, 0.039 mmol) in THF was refluxed for 10 h. The solvent was then removed in vacuo and the residue was subjected to TLC using *n*-hexane/CH<sub>2</sub>Cl<sub>2</sub> (6:1, *v/v*) as the eluent. Cluster **3** was obtained in 35% yield (*R*<sub>f</sub> = 0.55, 8.4 mg, 0.014 mmol), accompanied by a small amount of unchanged **2** (*R*<sub>f</sub> = 0.80, 1.0 mg, 0.0013 mmol, 5%).

**Reaction of Complex 3 with [Ru<sub>3</sub>(CO)<sub>12</sub>]:** Compound **3** (20 mg, 0.033 mmol) and a slight excess of [Ru<sub>3</sub>(CO)<sub>12</sub>] (15.4 mg, 0.024 mmol) were dissolved in *n*-octane or toluene (30 mL). The purple solution was heated to reflux for 4 h. The solvent was then removed under reduced pressure and the residue was subjected to TLC using *n*-hexane/CH<sub>2</sub>Cl<sub>2</sub> (6:1, *v/v*) as eluent. The first band contained [Ru<sub>3</sub>(CO)<sub>12</sub>] (*R*<sub>f</sub> = 0.95, 8.9 mg, 0.014 mmol). Two complexes were isolated in the following order of elution: [Ru<sub>6</sub>(μ<sub>3</sub>-H)(CO)<sub>12</sub>(μ-CO)(μ<sub>4</sub>-η<sup>2</sup>-CO)<sub>2</sub>(η<sup>5</sup>-C<sub>5</sub>Me<sub>5</sub>)]<sup>[34]</sup> (*R*<sub>f</sub> = 0.60, 3.8 mg, 0.0033 mmol, 10%) and cluster **3** (*R*<sub>f</sub> = 0.55, 6 mg, 0.0099 mmol, 30%).

**Thermolysis of 2 with PhC<sub>2</sub>Ph:** A solution of compound **2** (20 mg, 0.026 mmol) and diphenylacetylene (9.3 mg, 0.052 mmol) in *n*-octane (30 mL) was refluxed under argon atmosphere for 5 h. The complete consumption of **2** was indicated by spot TLC monitoring. After cooling, the solvent was evaporated in vacuo. Chromatography of the residue on silica eluting with *n*-hexane/dichlorome-

thane (2:1, *v/v*) afforded two major bands. Two consecutive bands were then eluted, containing [Ru<sub>3</sub>Co(CO)<sub>6</sub>(μ-CO)<sub>2</sub>(η<sup>5</sup>-C<sub>5</sub>Me<sub>5</sub>)(μ<sub>4</sub>-NH)(μ<sub>4</sub>-η<sup>2</sup>-PhC<sub>2</sub>Ph)] (**6**, *R*<sub>f</sub> = 0.40, 4.3 mg, 0.0047 mmol, 18%) and [Ru<sub>3</sub>Co(CO)<sub>5</sub>(μ-CO)<sub>2</sub>(η<sup>5</sup>-C<sub>5</sub>Me<sub>5</sub>)(μ<sub>4</sub>-η<sup>3</sup>-NC(O)C<sub>2</sub>(C<sub>4</sub>H<sub>4</sub>)CHCH(Ph))(μ<sub>4</sub>-η<sup>2</sup>-PhC<sub>2</sub>Ph)] (**7**, *R*<sub>f</sub> = 0.15, 1.7 mg, 0.0016 mmol, 6%). – C<sub>32</sub>H<sub>26</sub>NO<sub>8</sub>CoRu<sub>3</sub> (**6**, 914.7): calcd. C 42.01, H 2.84, N 1.53; found C 42.2, H 2.8, N 1.5. – C<sub>46</sub>H<sub>36</sub>NO<sub>8</sub>CoRu<sub>3</sub> (**7**, 1092.9): calcd. C 50.55, H 3.30, N 1.28; found C 50.7, H 3.2, N 1.4.

**Reaction of [Ru<sub>3</sub>Co(CO)<sub>12</sub>(μ<sub>4</sub>-N)] with [Cp\*Co(CO)<sub>2</sub>]:** A suspension of [Ru<sub>3</sub>Co(CO)<sub>12</sub>(μ<sub>4</sub>-N)] (100 mg, 0.14 mmol) and two equivalents of [Cp\*Co(CO)<sub>2</sub>] (70.2 mg, 0.28 mmol) in THF was refluxed. The resulting solution gradually changed from orange to dark-brown. Thermolysis was continued until no starting materials remained (about 4 h, as confirmed by IR spectroscopy). The mixture was then concentrated to dryness in vacuo. The dark-brown residue was redissolved in CH<sub>2</sub>Cl<sub>2</sub> (2 mL) and TLC separation (*n*-hexane/dichloromethane, 9:1, *v/v*) afforded [Ru<sub>2</sub>Co<sub>2</sub>(CO)<sub>9</sub>(η<sup>5</sup>-C<sub>5</sub>Me<sub>5</sub>)(μ<sub>4</sub>-N)] **8** (*R*<sub>f</sub> = 0.80, 32.4 mg, 0.045 mmol, 32%) and cluster **3** (*R*<sub>f</sub> = 0.48, 35.0 mg, 0.058 mmol, 41%). – C<sub>19</sub>H<sub>15</sub>NO<sub>5</sub>Co<sub>2</sub>Ru<sub>2</sub> (**8**, 721.3): calcd. C 31.62, H 2.08, N 1.94; found C 31.8, H 2.2, N 1.8.

### Electrochemical Studies

Electrochemical measurements were carried out using an EG & G Princeton Applied Research (PAR) Model 273A potentiostat/galvanostat connected to an interfaced computer employing PAR 270 electrochemical software. Cyclic voltammograms were obtained using a gas (argon) sealed two-compartment cell equipped with a glassy carbon working electrode (Bioanalytical), a platinum wire auxiliary electrode (Aldrich), and an Ag/AgNO<sub>3</sub> reference electrode (Bioanalytical) at room temperature; 0.1 mol dm<sup>-3</sup> *n*-tetrabutylammonium hexafluorophosphate (TBAHFP) in anhydrous deoxygenated CH<sub>2</sub>Cl<sub>2</sub> was used as a supporting electrolyte. Ferrocene was added at the end of each experiment as an internal standard.<sup>[80]</sup> Potential data (vs. Ag/AgNO<sub>3</sub>) were checked against the ferrocene (0/+1) couple; under the actual experimental conditions the ferrocene/ferrocenium couple is located at +0.18 V. Bulk electrolyses

Table 9. Crystal data and data collection parameters for compounds **2–6**

	<b>2</b>	<b>3</b>	<b>4</b>	<b>5</b>	<b>6</b>
Empirical formula	C <sub>19</sub> H <sub>16</sub> NO <sub>9</sub> CoRu <sub>3</sub>	C <sub>17</sub> H <sub>16</sub> NO <sub>7</sub> CoRu <sub>2</sub>	C <sub>22</sub> H <sub>17</sub> NO <sub>12</sub> Ru <sub>5</sub>	C <sub>42</sub> H <sub>46</sub> NO <sub>12</sub> CoRu <sub>6</sub>	C <sub>32</sub> H <sub>26</sub> NO <sub>8</sub> CoRu <sub>3</sub>
Formula weight	764.48	607.39	992.73	1422.18	914.70
Crystal colour, habit	Brown, block	Purple, block	Red, block	Green, block	Brown, prism
Crystal dimensions/mm	0.23 × 0.24 × 0.26	0.15 × 0.22 × 0.23	0.18 × 0.21 × 0.24	0.13 × 0.15 × 0.20	0.23 × 0.22 × 0.24
Crystal system	Triclinic	Monoclinic	Monoclinic	Monoclinic	Monoclinic
Space group	<i>P</i> 1̄ (no. 2)	<i>P</i> 2 <sub>1</sub> / <i>n</i> (no. 14)	<i>C</i> 2/ <i>c</i> (no. 15)	<i>P</i> 2 <sub>1</sub> / <i>c</i> (no. 14)	<i>P</i> 2 <sub>1</sub> / <i>c</i> (no. 14)
<i>a</i> /Å	10.963(1)	8.632(1)	31.589(2)	20.685(2)	10.405(1)
<i>b</i> /Å	9.843(5)	17.702(2)	10.324(1)	11.785(1)	18.875(1)
<i>c</i> /Å	12.027(4)	13.582(1)	19.549(2)	20.782(2)	16.199(1)
<i>α</i> /°	86.72(3)				
<i>β</i> /°	105.06(4)	97.78(2)	114.28(2)	111.01(2)	99.27(1)
<i>γ</i> /°	85.67(7)				
<i>V</i> /Å <sup>3</sup>	1245.7(8)	2056.3(4)	5811(1)	4729.3(10)	3139.8(4)
<i>Z</i>	2	4	8	4	4
Density (calcd.)/g cm <sup>-3</sup>	2.038	1.962	2.269	1.997	1.935
μ(Mo- <i>K</i> <sub>α</sub> )/cm <sup>-1</sup>	24.85	22.85	25.99	22.65	19.87
Diffractometer	Rigaku AFC7R	MAR Research Image Plate	MAR Research Image Plate	MAR Research Image Plate	MAR Research Image Plate
Reflections collected	3463	17185	25154	39075	28865
Unique reflections	3257	3658	5628	5275	5610
Obsd. reflections [ <i>I</i> > 1.5σ( <i>I</i> )]	2946	2857	3970	2950	3943
<i>R</i>	0.023	0.034	0.058	0.062	0.082
<i>R</i> '	0.028	0.047	0.062	0.056	0.090
Goodness of fit, <i>S</i>	1.85	1.65	2.21	1.37	1.63



Table 10. Crystal data and data collection parameters for compounds 7–8

	7·0.5CH <sub>2</sub> Cl <sub>2</sub>	8
Empirical formula	C <sub>46.5</sub> H <sub>37</sub> NO <sub>8</sub> ClCoRu <sub>3</sub>	C <sub>19</sub> H <sub>15</sub> NO <sub>9</sub> Co <sub>2</sub> Ru <sub>2</sub>
Formula mass	1135.40	721.34
Crystal colour, habit	Dark brown, prism	Brown, block
Crystal dimensions/mm	0.21 × 0.22 × 0.26	0.28 × 0.25 × 0.22
Crystal system	Monoclinic	Triclinic
Space group	P2 <sub>1</sub> /c (no. 14)	P1̄ (no. 2)
a/Å	16.205(1)	9.627(1)
b/Å	13.378(1)	10.707(1)
c/Å	20.673(2)	11.974(1)
a/°		75.31(2)
β/°	93.20(2)	88.64(1)
γ/°		92.35(1)
V/Å <sup>3</sup>	4474.7(6)	1192.1(2)
Z	4	2
Density (calcd.)/g cm <sup>−3</sup>	1.685	2.009
μ (Mo-Kα)/cm <sup>−1</sup>	14.70	26.58
Diffractometer	MAR Research Image Plate	MAR Research Image Plate
Reflections collected	40930	11539
Unique reflections	6558	4003
Obsd. reflections [I > 1.5σ(I)]	3697	3184
R	0.062	0.044
R'	0.055	0.050
Goodness of fit, S	1.52	1.66

were carried out in a gas-tight cell consisting of three chambers separated at the bottom by fine frits, with a carbon cloth (80 mm<sup>2</sup>) working electrode in the middle, and Ag/AgNO<sub>3</sub> reference and Pt gauze auxiliary electrodes in the lateral chambers. The working potentials ( $E_w$ ) for reduction and oxidation processes were ca. 0.15 V more negative and more positive than the corresponding electrode potentials ( $E_p$ ), respectively; all coulometric experiments were performed in duplicate.

### Crystallography

Crystals suitable for X-ray analyses were glued onto glass fibres with epoxy resin or sealed in 0.3 mm glass capillaries. Intensity data were collected at ambient temperature on either a Rigaku-AFC7R diffractometer (complex **2**) or a MAR research image plate scanner (complexes **3–8**) using graphite-monochromated Mo-K $\alpha$  radiation ( $\lambda = 0.71073$  Å) in the  $\omega - 2\theta$  and  $\omega$  scan modes, respectively. Details of the intensity data collection and crystal data are given in Table 9 and Table 10. The diffracted intensities were corrected for Lorentz and polarization effects. The  $\Psi$  scan method was employed for semiempirical absorption corrections in the case of **2**,<sup>[81]</sup> while an approximate absorption correction based on inter-image scaling was applied in the case of **3–8**. Scattering factors were taken from ref.<sup>[82]</sup> and anomalous dispersion effects<sup>[83]</sup> were included in  $F_c$ . The structures were solved by direct methods (SIR-92<sup>[84]</sup> for **6–8**; SHELX-86<sup>[85]</sup> for **2–5**) and expanded by Fourier-difference techniques. Atomic coordinates and thermal parameters were refined by full-matrix least-squares analysis on  $F_o$  with the ruthenium atoms and non-hydrogen atoms being refined anisotropically whenever possible. The nitrene and metal hydride hydrogens were located by Fourier-difference synthesis, while those of the organic moieties were generated in their ideal positions (C–H 0.95 Å). Calculations were performed on a Silicon Graphics computer, using the program package TEXSAN.<sup>[86]</sup>

Crystallographic data (excluding structure factors) for the structures reported in this paper have been deposited with the Cambridge Crystallographic Data Centre (CCDC) as supplementary publication nos. CCDC 149061–149067. Copies of the data can be

obtained free of charge on application to the CCDC, 12 Union Road, Cambridge CB2 1EZ, U.K. [Fax: (internat.) +44 (0)1223/336033; E-mail: deposit@ccdc.cam.ac.uk].

### Acknowledgments

We gratefully acknowledge financial support from the Hong Kong Research Grants Council and the University of Hong Kong. E. N.-M. Ho acknowledges the receipt of a postgraduate studentship, Swire Scholarship 1998–2000, Hung Hing Ying Scholarship 1998–2000, and Epson Foundation Scholarship 2000–2001 administered by the University of Hong Kong and Michael Gale Scholarship 1998–99 awarded by the University of Hong Kong and Hong Kong Telecom Foundation.

- [1] D. E. Fjare, D. G. Keyes, W. L. Gladfelter, *J. Organomet. Chem.* **1983**, 250, 383.
- [2] D. E. Fjare, W. L. Gladfelter, *J. Am. Chem. Soc.* **1984**, 106, 4799.
- [3] M. L. Blohm, W. L. Gladfelter, *Organometallics* **1985**, 4, 45.
- [4] A. Gourdon, Y. Jeannin, *J. Organomet. Chem.* **1992**, 440, 353.
- [5] M. L. Bedard, A. D. Rae, L. F. Dahl, *J. Am. Chem. Soc.* **1986**, 108, 5924.
- [6] W. L. Gladfelter, *Adv. Organomet. Chem.* **1985**, 24, 41.
- [7] W. Sun, S. Yang, H. Wang, Y. Yin, *Polyhedron* **1992**, 11, 1143.
- [8] C. E. Anson, J. P. Attard, B. F. G. Johnson, J. Lewis, J. M. Mace, D. B. Powell, *J. Chem. Soc., Chem. Commun.* **1986**, 1715.
- [9] A. Gourdon, Y. Jeannin, *Organometallics* **1986**, 5, 2406.
- [10] A. Czaka, K. Aika, *Catal. Sci. Technol.* **1981**, 3, 87.
- [11] P. H. Emmett, *The Physical Basis for Heterogeneous Catalysis* (Eds.: E. Drauglis, R. I. Jaffe), Plenum Press, New York, **1975**, p. 3–34.
- [12] E. L. Muetterties, T. N. Rhodin, E. Bard, C. F. Brucker, W. R. Pretzer, *Chem. Rev.* **1979**, 79, 91.
- [13] E. N.-M. Ho, W.-T. Wong, *J. Chem. Soc., Dalton Trans.* **1998**, 4215.
- [14] E. N.-M. Ho, W.-T. Wong, *J. Chem. Soc., Dalton Trans.* **1998**, 513.
- [15] K. K.-H. Lee, W.-T. Wong, *J. Chem. Soc., Dalton Trans.* **1996**, 1707.
- [16] K. K.-H. Lee, W.-T. Wong, *Inorg. Chem.* **1996**, 35, 5393.
- [17] K. K.-H. Lee, W.-T. Wong, *J. Organomet. Chem.* **1995**, 503, 43.

- [18] R. E. Stevens, R. D. Guettler, W. L. Gladfelter, *Inorg. Chem.* **1990**, 29, 451.
- [19] R. E. Stevens, W. L. Gladfelter, *J. Am. Chem. Soc.* **1982**, 104, 6454.
- [20] J. Kiviaho, M. Reinikainen, M. K. Niemelä, K. Kataja, S. Jääskeläinen, *J. Mol. Cat. A: Chem.* **1996**, 106, 187.
- [21] M. Reinikainen, J. Kiviaho, M. Kröger, M. K. Niemelä, S. Jääskeläinen, *J. Mol. Cat. A: Chem.* **1997**, 118, 137.
- [22] T. Matsuzaki, Y. Sugi, H. Arakawa, K. Takeuchi, K.-I. Bando, N. Isogai, *Chem. Ind.* **1985**, 555.
- [23] G. Jenner, P. Andrianary, *J. Mol. Cat.* **1990**, 58, 307.
- [24] K.-I. Tominaga, Y. Sasaki, T. Watanabe, M. Saito, *Studies in Surface Science and Catalysis* **1998**, 114, 495.
- [25] M. Hidai, Y. Koyasu, M. Yokota, M. Orisaku, Y. Uchida, *Bull. Chem. Soc. Jpn.* **1982**, 55, 3951.
- [26] G. Jenner, *J. Mol. Cat. A: Chem.* **1995**, 96, 215.
- [27] F. Schwyer, P. Braunstein, C. Estournès, J. Guille, H. Kessler, J.-L. Paillaud, J. Rosè, *Chem. Commun.* **2000**, 1271.
- [28] K. K.-H. Lee, W.-T. Wong, *J. Organomet. Chem.* **1999**, 577, 323.
- [29] J. A. Smieja, R. E. Stevens, D. E. Fjare, W. L. Gladfelter, *Inorg. Chem.* **1985**, 24, 3206.
- [30] M. S. Ziebarth, L. F. Dahl, *J. Am. Chem. Soc.* **1990**, 112, 2411.
- [31] S.-H. Han, J.-S. Song, P. D. Macklin, S. T. Nguyen, G. L. Geoffroy, *Organometallics* **1989**, 8, 2127.
- [32] H. Beurich, H. Vahrenkamp, *Angew. Chem.* **1978**, 90, 915; *Angew. Chem. Int. Ed. Engl.* **1978**, 17, 863.
- [33] Y. Chi, L.-K. Liu, G. Huttner, L. Zsolnai, *J. Organomet. Chem.* **1990**, 390, 50.
- [34] E. Kolehmainen, K. Rissanen, K. Laihia, Z. A. Kerzina, M. I. Rybinskaya, M. Nieger, *J. Organomet. Chem.* **1996**, 524, 219.
- [35] M. L. Blohm, D. E. Fjare, W. L. Gladfelter, *Inorg. Chem.* **1983**, 22, 1004.
- [36] H.-G. Ang, K.-W. Ang, S.-G. Ang, A. L. Rheingold, *J. Chem. Soc., Dalton Trans.* **1996**, 3131.
- [37] B. F. G. Johnson, T. M. Layer, J. Lewis, P. R. Raithby, W.-T. Wong, *J. Chem. Soc., Dalton Trans.* **1993**, 973.
- [38] C. Z. Tu, R. C. William, J. R. Steven, *Organometallics* **1994**, 13, 3594.
- [39] J. S. Field, R. J. Haines, D. N. Smit, *J. Chem. Soc., Dalton Trans.* **1988**, 1315.
- [40] C. A. Tolman, *J. Am. Chem. Soc.* **1970**, 92, 2956.
- [41] B. Ulf, M. Götz, S.-E. Helen, S.-F. Georg, *J. Chem. Soc., Dalton Trans.* **1992**, 2131.
- [42] R. D. Adams, J. E. Babin, M. Tasi, T. A. Wolfe, *J. Am. Chem. Soc.* **1988**, 110, 7093.
- [43] R. D. Adams, J. E. Babin, M. Tasi, *Organometallics* **1988**, 7, 503.
- [44] J. R. Galsworthy, C. E. Housecroft, R. L. Ostrander, A. L. Rheingold, *J. Organomet. Chem.* **1995**, 492, 211.
- [45] S. A. R. Knox, B. R. Lloyd, A. G. Orpen, J. M. Vinas, M. Weber, *J. Chem. Soc., Chem. Commun.* **1987**, 1498.
- [46] S. A. R. Knox, B. R. Lloyd, D. A. V. Morton, S. M. Nicholls, A. G. Orpen, J. M. Vinas, M. Weber, G. K. Williams, *J. Organomet. Chem.* **1990**, 394, 385.
- [47] B. F. G. Johnson, F. J. Lahoz, J. Lewis, N. D. Prior, P. R. Raithby, W.-T. Wong, *J. Chem. Soc., Dalton Trans.* **1992**, 1701.
- [48] M. L. Blohm, W. L. Gladfelter, *Organometallics* **1986**, 5, 1049.
- [49] J.-S. Song, S.-H. Han, S. T. Hguyen, G. L. Geoffroy, A. L. Rheingold, *Organometallics* **1990**, 9, 2386.
- [50] D. M. P. Mingos, D. J. Wales, *Introduction to Cluster Chemistry*, Prentice-Hall, New Jersey, **1990**.
- [51] Density functional calculations at the B3LYP level were performed on the model cluster  $[\text{Ru}_3\text{Co}(\text{CO})_6(\mu\text{-CO})_2(\eta^3\text{-C}_5\text{H}_5)(\mu_4\text{-NH})(\mu_4\text{-}\eta^2\text{-HC}_2\text{H})]$  on the basis of the experimentally determined geometry. The basis set used for C, N, O, and H atoms was 6-31G, while an effective core potential with a LANL2DZ basis set was employed for Ru and Co.
- [52] A. Reed, L. A. Curtiss, F. Weinhold, *Chem. Rev.* **1988**, 88, 899.
- [53] K. B. Wiberg, *Tetrahedron* **1968**, 24, 1083.
- [54] G. Schaftenaar, *Molden v3.5*, CAOS/CAMM Centre Nijmegen, Toernooiveld, Nijmegen (Netherlands), **1999**.
- [55] K. Wade, *Adv. Inorg. Chem. Radiochem.* **1976**, 18, 1.
- [56] Density functional calculations at the B3LYP level were performed on the model cluster  $[\text{Ru}_4(\text{CO})_9(\mu\text{-CO})_2(\mu_4\text{-NOH})(\mu_4\text{-}\eta^2\text{-HC}_2\text{H})]$  on the basis of the experimentally determined geometry. The basis set used for C, N, O, and H atoms was 6-31G, while an effective core potential with a LANL2DZ basis set was employed for Ru.
- [57] T. Jaeger, S. Aime, H. Vahrenkamp, *Organometallics* **1986**, 5, 245.
- [58] M. A. Collins, B. F. G. Johnson, J. Lewis, J. M. Mace, J. Morris, M. McPartlin, W. J. H. Nelson, J. Puga, P. R. Raithby, *J. Chem. Soc., Chem. Commun.* **1983**, 689.
- [59] E. Roland, H. Vahrenkamp, *Organometallics* **1983**, 2, 183.
- [60] J. S. Song, G. L. Geoffroy, A. L. Rheingold, *Inorg. Chem.* **1992**, 31, 1505.
- [61] K. Knoll, G. Huttner, T. Fassler, L. Zsolnai, *J. Organomet. Chem.* **1987**, 327, 255.
- [62] K. Knoll, G. Huttner, L. Zsolnai, O. Orama, *Angew. Chem.* **1986**, 98, 1099; *Angew. Chem. Int. Ed. Engl.* **1986**, 25, 1119.
- [63] K. Knoll, O. Orama, G. Huttner, *Angew. Chem.* **1984**, 96, 989; *Angew. Chem. Int. Ed. Engl.* **1984**, 23, 976.
- [64] G. Huttner, K. Knoll, *Angew. Chem.* **1987**, 99, 765; *Angew. Chem. Int. Ed. Engl.* **1987**, 26, 743.
- [65] R. D. Adams, J. A. Belinski, *Organometallics* **1991**, 10, 2114.
- [66] J. S. Haines, R. J. Haines, D. N. Smit, K. Natarajan, O. Scheidsteger, G. Huttner, *J. Organomet. Chem.* **1982**, 240, C23.
- [67] T. Jaeger, H. Vahrenkamp, *Z. Naturforsch.* **1986**, B41, 789.
- [68] D. Nuel, F. Dahan, R. Mathieu, *Organometallics* **1986**, 5, 1278.
- [69] G. D. Williams, G. L. Geoffroy, R. R. Whittle, A. L. Rheingold, *J. Am. Chem. Soc.* **1985**, 107, 729.
- [70] G. D. Williams, R. R. Whittle, G. L. Geoffroy, A. L. Rheingold, *J. Am. Chem. Soc.* **1987**, 109, 3936.
- [71] S. R. Drake, *Polyhedron* **1990**, 9, 455.
- [72] J. A. Page, G. Wilkinson, *J. Am. Chem. Soc.* **1952**, 74, 6149.
- [73] C. Furlani, E. O. Fischer, *Z. Elektrochem.* **1957**, 61, 481.
- [74] M. L. Blohm, D. E. Fjare, W. L. Gladfelter, *J. Am. Chem. Soc.* **1986**, 108, 2301.
- [75] M. Tachikawa, E. L. Muetterties, *J. Am. Chem. Soc.* **1980**, 102, 4541.
- [76] A. J. Gordon, R. A. Ford, *The Chemists Companion: A Handbook of Practical Data, Techniques, and References*, John Wiley & Sons, **1972**, p. 299.
- [77] D. E. Fjare, W. L. Gladfelter, *Inorg. Chem.* **1981**, 20, 3533.
- [78] R. E. Stevens, W. L. Gladfelter, *Inorg. Chem.* **1983**, 22, 2034.
- [79] L. R. Byers, L. F. Dahl, *Inorg. Chem.* **1980**, 19, 277.
- [80] G. Gritzner, J. Kute, *Pure Appl. Chem.* **1984**, 56, 461.
- [81] A. C. T. North, D. C. Phillips, F. S. Mathews, *Acta Crystallogr., Sect. A* **1968**, 24, 351.
- [82] D. T. Cromer, J. T. Waber, *International Tables for X-ray Crystallography*, Kynoch Press, Birmingham, **1974**, Vol. 4, Table 2.2B.
- [83] D. T. Cromer, J. T. Waber, *International Tables for X-ray Crystallography*, Kynoch Press, Birmingham, **1974**, Vol. 4, Table 2.3.1.
- [84] A. Altomare, M. C. Burla, M. Camalli, M. Cascarano, C. Giacovazzo, A. Guagliardi, G. Polidori, *J. Appl. Crystallogr.* **1992**, 25, 310.
- [85] G. M. Sheldrick, *Crystallographic Computing 3* (Eds: G. M. Sheldrick, C. Kruger, R. Goddard), Oxford University Press, **1985**, p. 175.
- [86] TEXSAN, Crystal Structure Analysis Package, Molecular Structure Corporation, Houston, TX, **1985** and **1992**.

Received October 13, 2000  
[I00389]